UNIVERSITY OF CALIFORNIA,
IRVINE

Estrogen Receptor Alpha Dynamics and Function in Mammalian Cells

THESIS

submitted in partial satisfaction of the requirements
for the degree of

MASTER OF SCIENCE

in Biomedical Engineering

by

Ramon Roca Pinilla

Thesis Committee:
Assistant Professor Michelle A. Digman, Chair
Professor Enrico Gratton
Professor Ellis R. Levin

2015

DEDICATION

To

my dear Dad, Mom, brother, and friends,

for their deep love, kindness and endless support.

In memory of Albert Armadans, for our friendship.

“PIPPIN: I didn't think it would end this way.

GANDALF: End? No, the journey doesn't end here. Death is just another path, one that we all must take. The grey rain-curtain of this world rolls back, and all turns to silver glass, and then you see it.

PIPPIN: What? Gandalf? See what?

GANDALF: White shores, and beyond, a far green country under a swift sunrise.

PIPPIN: Well, that isn't so bad.

GANDALF: No. No, it isn't.”

J.R.R Tolkien
“The Lord of The Rings”

TABLE OF CONTENTS

LIST OF FIGURES ..... **v**

ACKNOWLEDGMENTS ..... **vii**

ABSTARCT OF THESIS ..... **vii**

CHAPTER 1: Introduction **1**

1.1 Mechanism of Transcriptional Activation 2

1.2 Functional Roles of ERs in Physiology and Disease 4

1.3 Addressing unsolved biological questions by means of biophysical tools 6

CHAPTER 2: Analysis techniques **8**

2.1 Single Plane Illumination Microscopy for fluorescence microscopy 8

2.2 Fluorescence fluctuation techniques 9

2.2.1 Spatio-temporal image correlation (STICs) and Pair Correlation Function (pCF) to study molecular diffusion 10

2.2.2 pCF mathematical background for diffusion of particles 10

2.3 Binding Map 13

2.4 Fluorescence Lifetime Imaging Microscopy 15

2.4.1 Two component resolution 18

2.5 Number and Brightness 15

CHAPTER 3: Materials and Methods **22**

CHAPTER 4: Results **26**

4.1 From fast imaging to protein dynamics 26

4.2 ERα diffusion detection inside Live Cell Nuclei 28

4.3 Retrieving the nuclear topology from the binding map technique 32

4.4 ERα concentration-dependent localization 34

4.5 In vivo single-cell detection of metabolic pathways in breast cancer cells 40

CHAPTER 5: Discussion **43**

5.1 pCF and Binding Map 43

5.2 N&B 46

5.3 FLIM 47

CHAPTER 6: Conclusions and future directions **49**

6.1 Conclusions 49

6.2 Future directions 50

BIBLIOGRAPHY **51**

APPENDIX A: Simulations and N&B mathematical background **54**

LIST OF FIGURES

Figure 1: Schematic representation of the domain structure of the estrogen receptors(ERs) **1**

Figure 2: Illustrative representation of the estrogen receptor..... **2**

Figure 3: Schematic representation of the ERα functions depending on the cellular compartments..... **4**

Figure 4: Picture of the selective plane illumination microscope **9**

Figure 5: The pair correlation function (pCF) approach **13**

Figure 6: Schematic representation of the theory behind the binding map technique **15**

Figure. 1: Schematic representation for the FLIM-Phasor approach **19**

Figure. 8: Schematic of the SPIM setup sample mounting..... **25**

Figure. 9: pCF analysis of the stack of images of live CHO-k1 cell nuclei..... **27**

Figure. 10: pCF analysis in live cell nuclei **28**

Figure. 11: Time dependence of the diffusion coefficients **30**

Figure. 12: Mean diffusion values **31**

Figure. 13: Binding Map **33**

Figure. 14: ERα in CHO-K1 cells..... **35**

Figure. 15: ERα subcellular localization as a function of concentration..... **36**

Figure. 16: ERα concentration in different subcellular compartments..... **37**

Figure. 17: Effect of different hormone concentrations **39**

Figure. 18: Metabolic plasticity in MCF-7 breast cancer cell lines **41**

Figure. 19: Mathematical transformation of fluorescence decay raw data **42**

Figure. 20: Simulated correlation functions.....45

Figure. 21: N&B mathematical background.....56

ACKNOWLEDGMENTS

I would like to express the deepest appreciation to my committee members, Professor Michelle Digman, Professor Enrico Gratton, and Professor Ellis Levin for all the help and knowledge. Their profound teaching and support has left me with a great research experience.

I would like to thank Carmine Di Rienzo, Jenu Chacko, Hongtao Chen, Milka Stakic, and Nik Hedde for their help and suggestions as well as guiding me through the obstacles faced throughout the project.

I would also like to thank my labmates, Michael Murata, Andrew Trinh, Swathi Bagilthaya, Emma Mah, Jenu Chako and Ning Ma for making every day in lab more enjoyable.

ABSTRACT OF THE THESIS

Estrogen Receptor Alpha Dynamics and Function in Mammalian Cells

By

Ramon Roca Pinilla

Master of Science in Biomedical Engineering

University of California, Irvine, 2015

Professor Michelle A. Digman, Chair

The role of estrogen receptors (ER) is highly dependent on their sub-cellular localization and concentration. Here, we propose an approach to detect molecular transport, diffusion and localization of the estrogen receptor α by measuring the time cross-correlation between pairs of locations and the average number of molecules by means of fluorescence fluctuations in mammalian cells. From this data we find that there is concentration dependence for the localization of the estrogen receptor and that 17-β-Estradiol (E2) reduces the apparent diffusion of the receptor. In addition, we use fluorescence lifetime imaging, a label-free, non-invasive imaging method to demonstrate changes in the glucose metabolic pathway in ER-positive breast cancer cells. We observe a higher free to bound NADH ratio in high glucose conditions, reflecting and increased glycolysis/oxidative phosphorylation ratio. Furthermore, E2 is able to potentiate metabolic adaptation and cell viability depending on the glucose availability. Taking advantage of a wide array of available biophysical analysis techniques may provide additional useful information for estrogen receptors and in breast cancer research.

Chapter 1 Introduction

Estrogen and its receptors (ERs) play important roles in the development and maintenance of normal sexual and reproductive function, with a vast range of biological effects in the cardiovascular, musculoskeletal, immune, and central nervous system[1]. Moreover, they are also crucial in the genesis and malignant progression of breast cancer[2].

ERs are ligand-activated transcription factors that can bind 17-β-estradiol, the most potent estrogen produced in the body. The first ER was cloned in 1986 and was regarded as the only receptor until a second ER was reported in 1996. The two receptors, known today as ERα and ERβ, show a high degree of similarity when their respective amino acid sequences are compared. The sequence homology is approximately 97% in the DNA-binding domain and approximately 56% in the ligand-binding domain, whereas at the N terminus the homology is only 24%[1,3] (Fig. 2, Fig. 3)

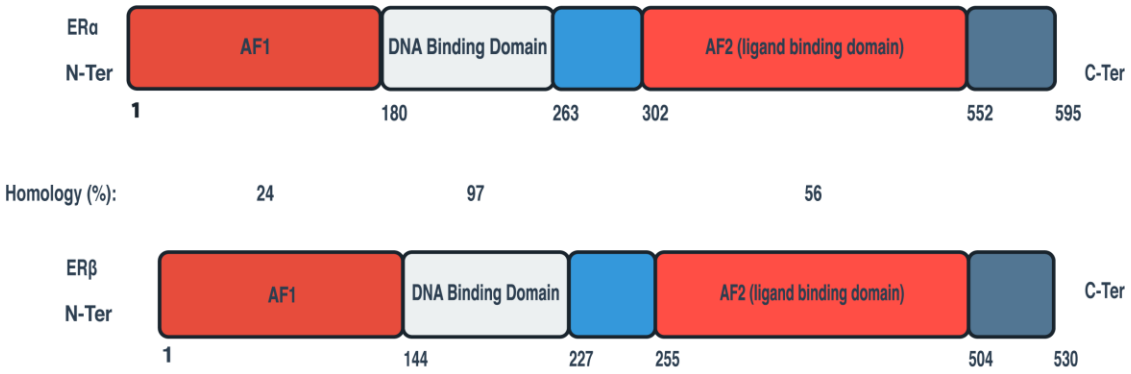

Fig. 2 Schematic representation of the domain structure of the estrogen receptors (ERs).

Transcriptional activation by ERα is mediated by two distinct activation functions (AF): the constitutively active AF-1 in the N-terminal domain of the receptor and the ligand-dependent[4] AF-2, located in the C-terminal domain of the receptor protein. When compared, ERβ has a weaker AF-1 function, hence depending more on the ligand-dependent action of AF-2 for its transcriptional activation function. The relative importance of the AF-1 and AF-2 activation functions depends on cellular and promoter context[4,5].

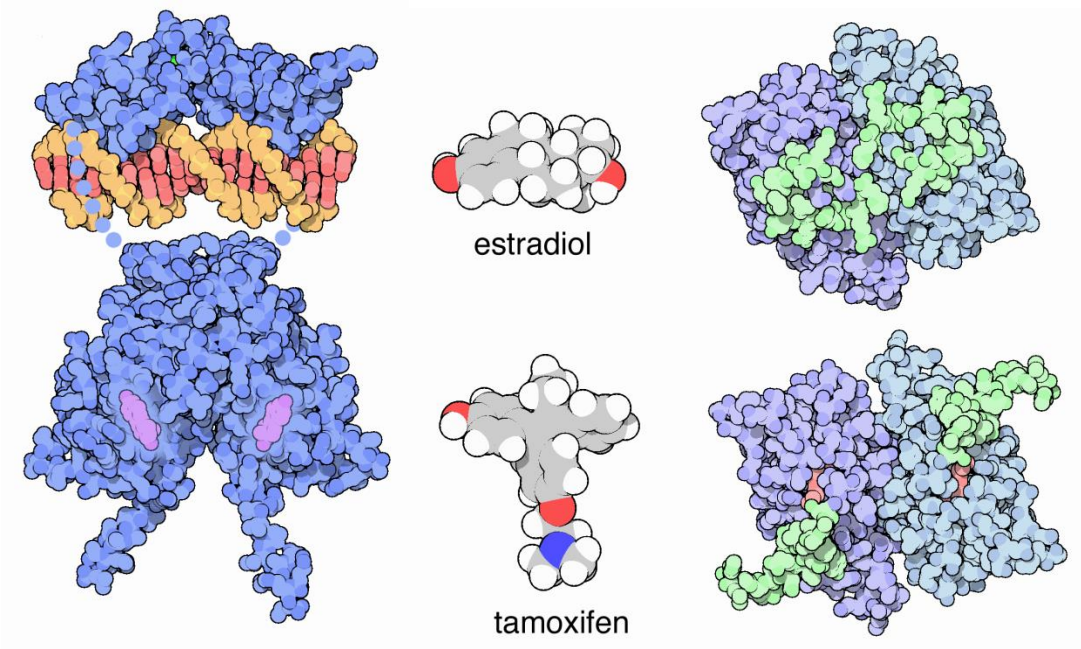

Fig. 3. Illustrative representation of the estrogen receptor, its interaction with the DNA, ligands and ligand-dependent adopted conformations[6].

1.1 Mechanism of Transcriptional Activation

Estrogens are small, carbon-rich molecules built from cholesterol. Contrary to larger hormones, such as insulin and growth hormone, which are sensed by receptors on the cell

surface, estrogens can also pass directly into cells throughout the body into the nucleus, right at the site of action on DNA[6].

Like other steroid hormone receptors, ERs act as dimers, upon hormone binding, to regulate transcriptional activation. ER activated transcriptional control requires interaction with coregulator complexes, either coactivators or corepressors of the target gene expression. The consensus estrogen response element (ERE; GGTCAnnnTGACC) is required for some estrogen responsive genes, although most of the regulated genes do not contain this perfect palindromic consensus sequence. In addition, ERs can bind other transcription factors and activate them in order to trigger transcription indirectly. Selective action of ERs in vivo is probably a result of the complex interplay at a given time point between expression levels of each ER type, the relative affinity for a specific promoter, ligand and cofactor availability, and interaction with other transcription factors. A significant number of post-translation modifications, such as phosphorylation, SUMOylation, ubiquitination, acetylation or palmitoylation of ERs have also been described, affecting the receptor activity, stability and localization in sub-cellular compartments[7].

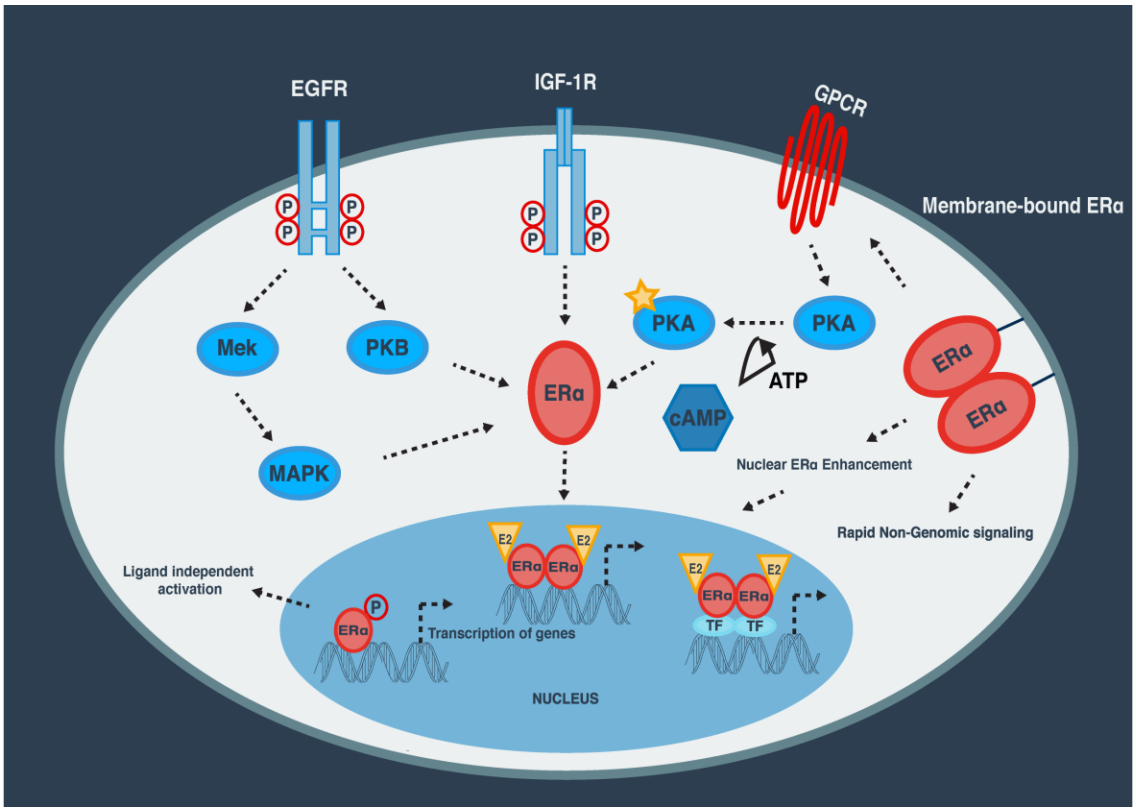

Fig. 4 Schematic representation of the ERα functions depending on the cellular compartment[1,7,8].

1.2 Functional Roles of ERs in Physiology and Disease

Estrogens gives cells permission to grow when required. This is essential during puberty, but also necessary during adult life[6].

Estrogens and other selective estrogen-receptor modulators (SERMs), molecules that mimic the shape of estrogen and bind tightly to the estrogen receptor, such as Tamoxifen or Fulvestrant, exert effects on multiple organs. For example, Tamoxifen is larger than the hormone forcing ER into an inactive conformation and therefore blocking the signal to grow (Fig. 3).

It is generally believed that breast tumors depend, at least initially, on the stimulatory effects of estrogens for their development[1,4,5,9]. However many breast tumors eventually progress to an estrogen-independent growth phenotype. Tamoxifen and similar antiestrogens are currently in the first-line therapy for treatment of hormone-dependent breast cancers. Normal and cancer tissues display a variety of distinct profiles regarding the ER isoform and splice variants at both mRNA and protein levels. This heterogeneity is suggested to result in variation in estrogen signaling, therefore affecting breast cancer risk, treatment responsiveness and survival. Currently, only the ERα isoform is clinically measured for clinical decision-making and treatment[9].

It is important to note that ERs play an important role in other types of cancers and other diseases. Prostate cancer is the most frequently diagnosed malignancy and the second most common cause of death among men in the United States. In this case, both androgens and estrogens play an important role. Estrogens also exert a cardio-protective role by reducing circulating lipid levels and by enhancing NO production, necessary for endothelium-dependent peripheral vasodilatation. Moreover, estrogen and its receptors are known to be important in the regulation of bone metabolism. Estrogen deficiency beginning at menopause is a major pathogenic factor in the development of osteoporosis in post-menopausal women. Finally, estrogens and ERs are implicated in various disorders of the brain or in metabolic diseases, such as reduction of the adipose tissue by increasing lipolysis or protection against insulin resistance[8,9]. However, little information exists on a role for estrogen receptor diffusion and how estradiol affects its transport and interactions, from a biophysical perspective.

Previous studies are based on single point fluorescence correlation spectroscopy (FCS) or fluorescence recovery after photobleaching (FRAP). FCS is a correlation analysis of temporal fluctuations on the fluorescence intensity that offers insight of diffusion behavior and absolute concentration of detected particles. FRAP is a technique capable of quantifying diffusion by focusing light onto a small region of a viewable area. The fluorophores in this region receive high intensity illumination which causes fluorophores to bleach. As Brownian motion proceeds, the non-bleached molecules will diffuse through the sample and replace the non-fluorescent probes in the bleached region. Therefore, transport can be quantified with bot these techniques[10]. However, FRAP is an invasive techniques and both these methods suffer in terms of spatial resolution[11–13]. Moreover, imaging techniques are needed not only to retrieve diffusion but also to quantify cellular localization and function of the estrogen receptor. Here, we introduce different fluorescence imaging-based techniques in order to address some of these questions in mammalian cells.

1.3 Addressing unsolved biological questions by means of biophysical tools

In this particular study, additional information regarding the ERα is provided using a biophysical approach, in contrast to traditional biochemical studies. One specific aim of our research is to retrieve dynamics, localization and structural characteristics in mammalian cells. This is achieved by measuring protein transport and localization in a quantitative way using fluorescence fluctuation techniques[14–16]. In addition, drug-induced perturbations that affect protein transport and interaction can be evaluated.

Another aim of the research is to acquire metabolic information through fluorescence lifetime imaging (FLIM) analysis of live mammalian cells. FLIM can be a useful asset in order to asses a broad spectrum of different metabolic states[17–19]. However, the scope of the present research is focused on metabolic plasticity for breast cancer cells under different glucose availability. These variable substrate concentrations are representative of the *in-vivo* microenvironment that tumor cells may be exposed to. Finally, FLIM can also address the effect of E2 in order to potentiate breast cancer adaptation to different energetic constraints[20]. Capitalizing on non-invasive imaging techniques might provide additional means for diagnosis and consequently better treatments. All of the techniques are explained in the following chapters.

Chapter 2 Analysis techniques

2.1 Single Plane Illumination Microscopy for fluorescence microscopy

The ability to measure biomolecular dynamics is critical for unveiling fundamental physiological processes within live cells such as cell adhesion, signaling, movement, division or metabolism[15].

In that regard, we show that the combination of fluorescence fluctuation microscopy techniques (described in sections 2.2) together with single plane illumination (SPIM) data is a fast and more efficient way of unraveling rapid molecular transport and interactions in living cells. In SPIM, excitation and detection of fluorescent samples are decoupled by the use of two objective lenses arranged perpendicular to each other (Fig. 5). A thin sheet of light from the excitation objective limits fluorescence emanating from the focal plane, allowing for optical sectioning of live samples. Moreover, light exposure levels are very low, thus reducing cytotoxicity. Therefore, the custom made SPIM setup allows fluorophores in the nucleus of living cells to be selectively excited (Fig. 5). Finally, the technique employed does not require calibration of the Point Spread Function (PSF) (see 2.4). [15].

For the quantification of protein dynamics, first, a stack of camera images recorded in the order of milliseconds is obtained. Then, these recorded acquisitions are correlated as explained in section 2.2 (**Error! Reference source not found.**). Hence, the diffusion vs. time plot is obtained[14,15].

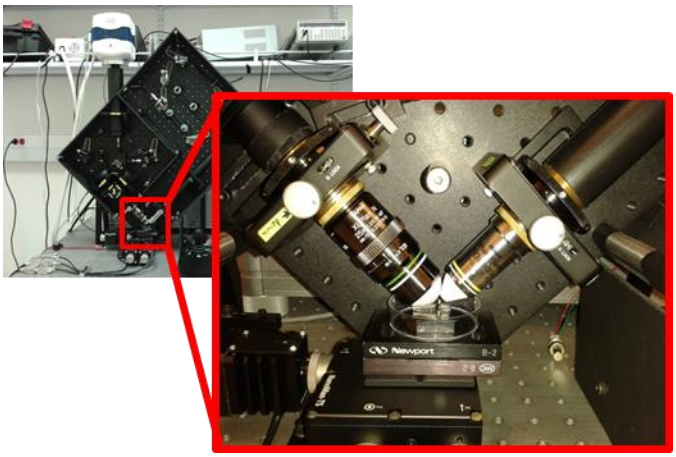

Fig. 5. Picture of the selective plane illumination microscope. The SPIM system is setup using a vertical breadboard secured onto an optical anti-vibration table. It is a home-build microscope by Dr. Nik Hedde at the laboratory of fluorescence dynamics (LFD), University of California Irvine (UCI).For exciting green fluorescence, a 488-nm laser diode (488 nm, ISS, Champaign, IL, USA) is used. The green channel is imaged onto the chip of an sCMOS camera(Zyla 4.2, Andor, Belfast, North Ireland).The inset shows the two objective lenses dipping into the sample dish as described in materials and methods[15].

2.2 Fluorescence fluctuation techniques

In living systems homeostasis is achieved by a complex landscape of precisely regulated interactions. These interactions control the localization of the molecular constituents within the cell at any given time point. Therefore, tracking fluorescent probes such as green fluorescent protein (GFP) within the cellular environment allows for the application of fluorescence fluctuation techniques. Fluorescence fluctuation microscopy includes a broad array of analytical tools that provide quantitative information of cellular structures, their organization and the intrinsic molecular dynamics.

Fluctuating fluorescence signal that derives from adequately labeled reporters allow for non-invasive measurements of diffusion coefficients, binding constants, concentrations, oligomerization and other parameter in live samples. These parameters can be obtained over

many microns in the sample, and can reveal the variation in response to certain treatments such as hormones (e.g. 17-β-Estradiol).

Thus, within the constraints imposed by the required fluorescence labeling, fluctuation microscopy has the potential to add a dynamic molecular element to standard fluorescence imaging *in vitro* and *in vivo*.

2.2.1 *Spatio-temporal image correlation (STICs) and Pair Correlation Function (pCF) to study molecular diffusion*

Within the context mentioned in 2.1 and 2.2, spatio-temporal image correlation microscopy, a technique based on fluorescence fluctuations, allows us to calculate the actual molecular diffusion directly from imaging. First, fast imaging of the region of interest is performed from which a stack of images is obtained. Each image in the stack is separated by a certain time delay. Subsequently, the pair correlation function is retrieved at certain radial distances as a function of time, starting from the center of the region of interest (Fig. 6).

The pair correlation function between the correlations at two points measures the time for a particle at a given point to appear at the second point[11]. A particle observed at time t= 0 at the origin will be found at a distance r_n with a probability proportional to the pair correlation function at a given distance. Notably, only the same particles will produce an average positive correlation at a given time delay at two different points[21]. Traditionally the pair correlation is performed along a line of pixels but not using 2D intensity images. However, this technique can

be applied to our data because in the SPIM microscope frames are acquired very fast (2ms) and to increase the signal to noise (S/N) in all the points equidistant to the origin are averaged.

The specific amount of time required to travel a distance is used to calculate a quantity proportional to the apparent diffusion coefficient for that particle.

It is important to remark that this approach can resolve average molecular dynamic properties well below the limit imposed by diffraction (~142 nm). *In silico* tests to demonstrate this approach are performed, through several simulated 2-D diffusion conditions, and in live cells, through a succession of fluorescently-labeled benchmark molecules (both protein and lipids). Furthermore, this approach does not require extraction of the individual trajectories of each one of the molecules.

Finally, it can be argued that this approach may represent a powerful tool in order to discover dynamic molecular properties that can be used to construct biophysical models to explain certain cell behaviors.

2.2.2 pCF mathematical background for diffusion of particles

The fluorescence intensity at any given time and position δr from the origin is given by[11]:

$$F(t,\delta r) = kQ\int W(r)C(r+\delta r,t)dr, \quad (1)$$

Where C(r,t) is the diffusion propagator, which can be interpreted as being proportional to the probability of finding a particle in position r and time t if the particle is at position 0 at time $t = 0$.

The mathematical description of C(r,t) is given by:

$$C(r,t) = \frac{1}{(4\pi Dt)^{3/2}} \cdot \exp\left(-\frac{r^2}{4Dt}\right) \quad (2)$$

Fluorescence is assumed to be proportional to the concentration, the quantum yield Q, filter combination excitation-emission laser power and the position of the particle in the profile of illumination $W(r)$. The pCF for two points at a distance δr as a function of the time delay τ is calculated by the following equation:

$$G(\tau,\delta r) = \frac{\langle F(t,0)\cdot F(t+\tau,\delta r)\rangle}{\langle F(t,0)\rangle\langle F(t,\delta r)\rangle} - 1 \quad (3)$$

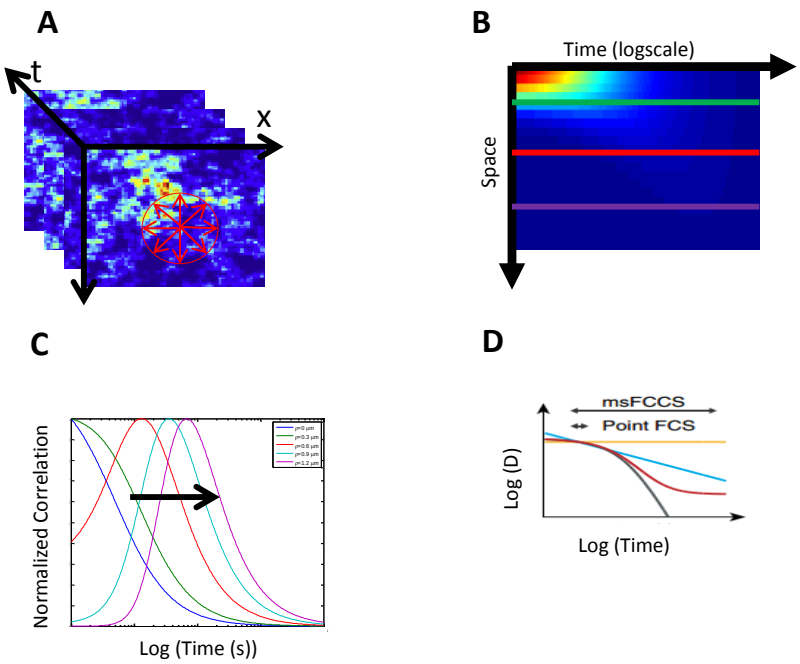

Fig. 6 The pair correlation function (pCF) approach (A) From a series of fluorescence images the spatiotemporal correlation is calculated. (B) At certain distances the pair correlation is retrieved as a function of time (green, red and purple lines) (C) Normalized pair correlation as a function of time. Each color represents a certain radial distance from the initial point $\boldsymbol{r_0}$, fixed by the pixel size (142 nm). (D) Diffusion as a function of time is obtained by the pCF approach. The time dependence of the diffusion coefficient reflects the nano-structural environment that conditions the protein movement.

2.3 Binding Map

A ubiquitous observation in cell biology us that the diffusive motion of macromolecules and organelles is anomalous. Therefore, descriptions based only on the conventional diffusion equation with diffusion constants measured in dilute solution fail to explain this particular behavior. Macromolecular crowding in the interior of the cells and in cellular membranes may be one of the possible explanations. One of the most common phenomenon that explains transport is a sub-linear, power law increase of the mean-square displacement (MSD). However, there are other types of manifestations such as time-dependent and strongly reduced diffusion coefficients, persistent correlations in time, non-Gaussian distributions of spatial

displacements, heterogeneous diffusion and the presence of a fraction of immobile particles[22]. There are several widely used theoretical models to describe transport in a heterogeneous environment. Notably, a particular emphasis is put in the spatiotemporal properties of the aforementioned transport in terms of how the different techniques explain transport. This can be done through two-point correlation (e.g. Pair Correlation Function (pCF)) functions or dynamic scaling behaviors, to mention some.

These theoretical models are then applied to experimental techniques based on fluorescence fluctuations, such as fluorescence correlation spectroscopy (FCS) and fluorescence recovery after photobleaching (FRAP) as explained in 1.2

In an effort to visualize dynamic observations in the nucleus of live cells in a topological fashion, the binding map technique was developed in our lab by Carmine Di Rienzo. The technique is still in a preliminary state and has not been published yet, but it consists of the following: for a stack of images, the technique retrieves the time delay between correlation functions (Fig. 7), at each pixel. Plotting the space vs. the time delay obtained at each pixel will give a linear curve with a certain slope (θ). If θ is >0 (θ_D), the particles are considered as "diffusive" at that particular pixel. On the contrary, if the slope is < 0 (θ_B), molecules are considered to be "bound" at that pixel. Hence, a map can be obtained that describes possible internal paths within a subcellular compartment for the molecule under study and regions of confinement along with the necessary obstacles and barriers for that to occur.

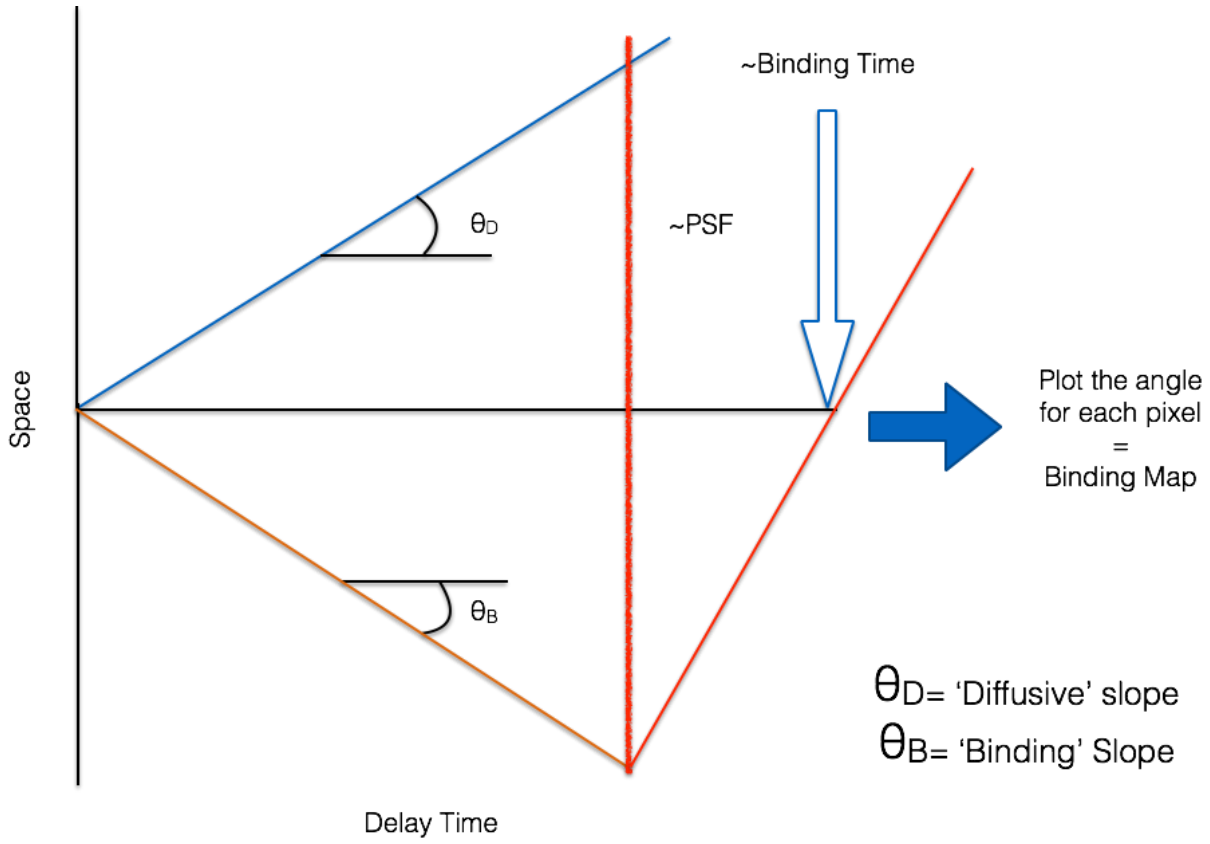

Fig. 7 Schematic representation of the theory behind the binding map technique. For each pixel a distance vs. delay time slope is obtained and plotted. If the slope for the obtained curve is > 0 ($\boldsymbol{\theta_D}$) (**blue line**), molecules are considered to be diffusing at that pixel. On the contrary, if the slope is < 0 ($\boldsymbol{\theta_b}$), molecules are considered to be bound at that pixel (orange line). However, bound molecules will diffuse eventually and the slope will be > 0 after a certain amount of delay time (thin red line). Thus, the intersection between the x-axis and the thin red line is approximately the binding time (white and blue arrow). The size of the PSF is approximately given by the distance between the blue and orange curves (thick red line).The binding map technique plots the corresponding slope ($\boldsymbol{\theta_D or\ \theta_b}$) at each pixel in a color map.

2.4 Fluorescence Lifetime Imaging Microscopy

The previous sections in this chapter discussed analysis techniques for the study of spatio-temporal dynamics of molecules inside living cells. These provide information about the local microenvironment within the nucleus for the ER receptor. To investigate alterations of metabolic changes upon stimulation with estrogen, it is necessary to use fluorescence lifetime imaging microscopy (FLIM) and measure the intrinsic autofluorescence signal derived from

nicotinamide adenine dinucleotide (NADH). Considering that different molecular species or different conformations of the same molecule have different lifetimes, the fluorescence decay can be measured using FLIM in the frequency domain, time-sampling approach, or time-correlated single photon counting[23].

The phasor approach, used in this study, has the potential of simplifying the analysis of FLIM images avoiding some of the problems of the exponential analysis and simultaneously providing a visual general view of the processes affecting the fluorescence that arises at each pixel[17–19]. The phasor method transforms the histogram of time delays at each pixel in a phasor diagram, which has the properties of a vector[17]. Moreover, the phasor plot is reciprocal. That means that each one of the points can be directly associated to the corresponding pixel of the image that generated it.

This two-dimensional histogram consists of the plot for the sine-cosine transforms of the following equations:

$$g_{i,j}(\omega) = \int_0^\infty I_{i,j}(t)\cos(\omega t)\,dt / \int_0^\infty I_{i,j}(t)dt \quad (4)$$

$$s_{i,j}(\omega) = \int_0^\infty I_{i,j}(t)\sin(\omega t)\,dt / \int_0^\infty I_{i,j}(t)dt \quad (5)$$

Where s and g are the coordinates in the phasor plot corresponding to a given fluorescent decay $I(t)$ andω is the laser repetition angular frequency or the angular frequency of light modulation. i and j indexes denote a specific pixel of an image. For data measure in frequency domain then:

$$g_{i,j}(\omega) = m_{i,j}\cos(\phi_{i,j}) \quad (6)$$

$$s_{i,j}(\omega) = m_{i,j}\sin(\phi_{i,j}) \quad (7)$$

Where $m_{i,j}$ and $\phi_{i,j}$ are the modulation and the phase of the emission with respect to the excitation, respectively.

For a single exponential decay $I(t) = A \cdot \exp\left(-\frac{t}{\tau}\right)$ the coordinates of the phasor plot are given by:

$$g_{i,j}(\omega) = \frac{1}{1 + (\omega\tau)^2} \quad (8)$$

$$s_{i,j}(\omega) = \frac{\omega\tau}{1 + (\omega\tau)^2} \quad (9)$$

If in at a given pixel i, j we have the contribution of several exponential ocmponents, the coordinates g and s of the phasor are given by:

$$g_{i,j}(\omega) = \sum_k \frac{f_k}{1 + (\omega\tau_k)^2} \quad (10)$$

$$s_{i,j}(\omega) = \sum_k \frac{f_k\omega\tau_k}{1 + (\omega\tau_k)^2} \quad (11)$$

Where f_k is the intensity weighted fractional component with lifetimeτ_k. According to the expressions for the coordinate of a phasor for a single exponential decay, $s_{ij}^2 + \left(g_{ij} - \frac{1}{2}\right)^2 = 1/4$, which implies that all single exponential components are represented within the limits of a semicircle of center $(\frac{1}{2}, 0)$ and radius $\frac{1}{2}$ in the phasor plot. Digman et al. named this circle the "universal circle"[17]. Short lifetimes (small phase angles) are close to the point $(1,0)$, whereas long lifetimes are close to the $(0,0)$ point.

2.4.1 Two component resolution

For the resolution of the fractional contribution of two phasor components Eq. 12 is solved graphically in the phasor plot. In this particular case, the phasors are along a segment where the extremes of the segment correspond to the phasor of the two isolated components (Fig. 8). Generally, the position of the isolated components is known or can be obtained empirically. When combined, the fractional contribution of each component is displayed on the screen and will determine the position along the mentioned segment.

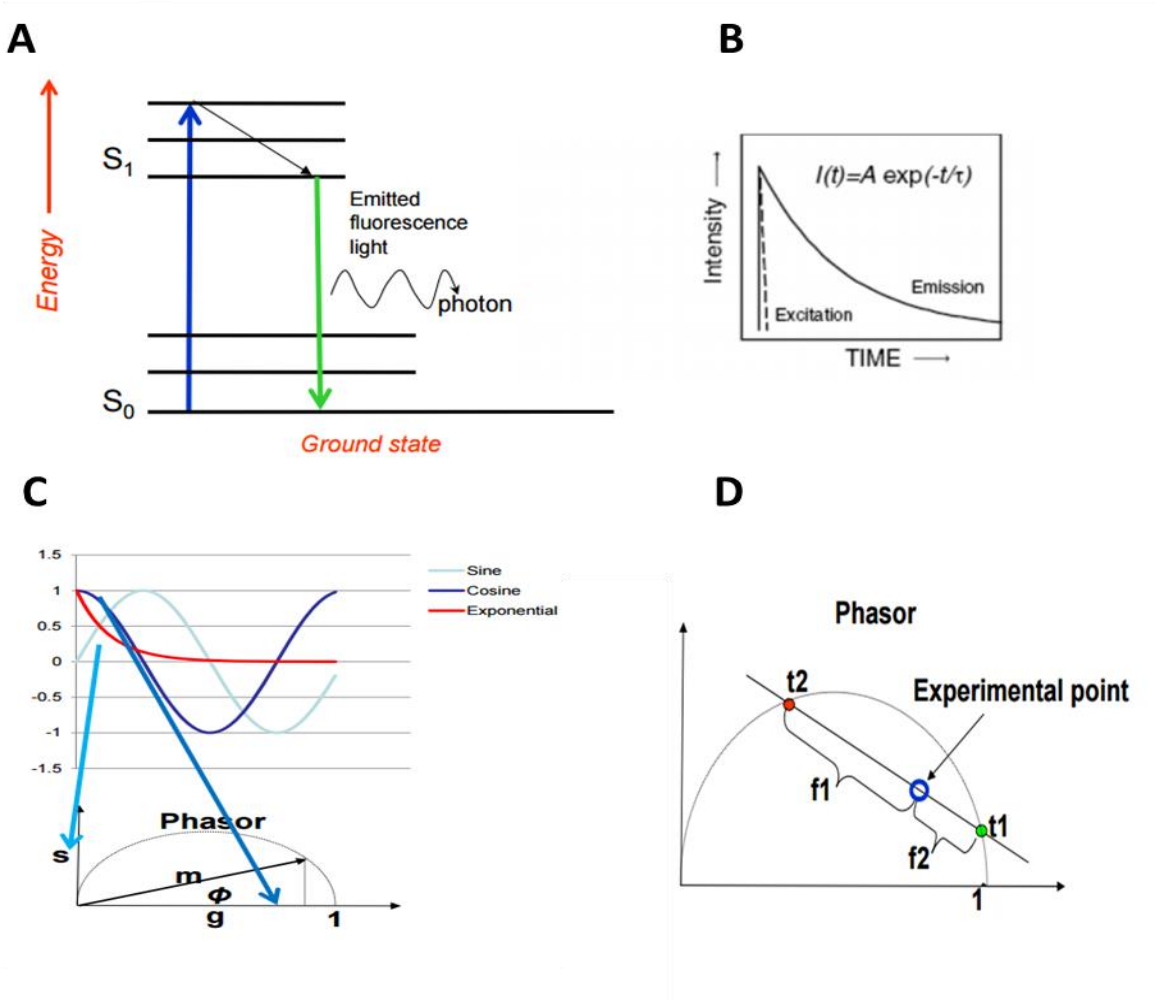

Fig. 8 Schematic representation for the FLIM-Phasor approach. (A) Jablonsky diagram that illustrates the electronic states of a molecules and the transitions between them. A fluorophore which is excited by a photon will drop to the ground state with a certain probability based on the decay rates, through a number of different decay pathways. The fluorescence emitted will decay as a function of time. (B) Lifetime decay after excitation of a fluorophore in the time domain after pulse excitation (C) The exponential lifetime decay can be processed mathematically to obtain the coordinates of the phasor plot. (D) The mixture of two components lay along the line that connects pure molecular species with lifetime t1 and t2, respectively in the phasor plot.

2.5 Number and Brightness

Classically, the ER is considered to mediate genomic as well as nongenomic responses under the presence of estradiol. In case of genomic responses, the ER acts as a ligand-dependent transcription factor that regulates gene expression in tissues. In contrast, non-genomic effects are generally though to start at the plasma membrane. This leads to rapid activation of cytoplasmic signal transduction pathways[7,24]. This suggests that the ER role is highly dependent on subcellular localization. However, the subcellular localization and roles for this receptor is still object of controversy to date[24].

Here, we suggest an image-based technique, named number and brightness (N&B), which allows for the detection of the subcellular localization of molecules such as the estrogen receptor. This technique is based on the measurement of the average number of molecules and brightness in each pixel in fluorescence microscopy images. The average brightness of a particle (e.g. a transcription factor labeled with an adequate fluorescent reporter, such as GFP) can be acquired from the ratio of the variance to the average intensity collected at each pixel. Moreover, the average number of fluctuating particles can be obtained by dividing the average intensity by the brightness at a given pixel[25].

This analysis can be used in a broad spectrum of concentrations and in live cells. In the particular case of live cells, the intensity at any given pixel may be due to bright but immobile structures, dim fast diffusing particles and to autofluorescence or scattering.

Furthermore, the variance of the detector noise is also added to the variance of the components mentioned above giving the total variance at each pixel, if all of the sources of variance are independent.

The fluctuation of particles in the volume of observation is proportional to the square of the particles brightness while the variance of the other components such as detector shot noise is proportional to the intensity of these components. Thus, only the fluctuations of the mobile particles (e.g. Transcription factor diffusion inside the nucleus) will have a ratio of the variance to the intensity higher than 1. In addition, changes in the fluorescence due to an intensity increase of the illumination power allows for the distinction of the different possible contributions. It is important to note, that in this particular study only the average number of ERα-GFP particles in three different subcellular compartments (nucleus, cytoplasm and membrane) was assessed. However, the precise oligomerization state was not assessed (Brightness part of the technique). Finally, N&B is a powerful tool for unveiling particle localization and concentration in live cells in order to help understand protein function and signaling as a function of the concentration dependent localization of proteins.

Chapter 3 Materials and Methods

SPIM imaging and data processing. Fluorescence images were acquired with a custom-built SPIM setup running Micro-Manager (available at www.micro-manager.org). STICS correlation and pCF analysis were performed with custom Matlab (MathWorks, Natick, Massachusetts, USA) scripts. Data was visualized with SimFCS, Matlab and Origin (OriginLab, Northampton, USA).

N&B imaging and data processing. Fluorescence images were acquired with a commercial Olympus Fluoview 1000 (FV1000) laser scanning microscope. Instrumental PSF was calibrated using subdiffraction-sized fluorescent beads and found to be at ~270 nm for 488-nm excitation wavelength. Images were obtained by illumination of the sample with a 488-nm laser, using a 60x (N.A. 1.20) water immersion objective to collect fluorescence. Each image consists of the average intensity of 10 frames using a Kalman filter. The data consists of intensity images that are analyzed with custom made MatLab code.

FLIM image and data processing. Lifetime measurements were carried out with a Zeiss 710 microscope coupled to a Ti:sapphire laser system(Spectra-Physics Mai Tai). A 40 x (0.8 N.A) water immersion objective was used. The excitation wavelength was 740 nm with an average power of ~5 mW. Fluorescence intensity images of NADH were acquired by exciting the cells at 740 nm and placing a 460/80 nm emission filter in front of the detector. Fluorescence lifetime images were acquire with an ISS A320 FastFLIM system[26]. For image acquisition the following setting were used: 256 x 256 pixels images and a laser scan speed of 25 μs/pixel. A dichroic filter (690 nm) was used to separate the fluorescence signal from the laser light signal.

Fluorescence is detected by a photomultiplier (H&422P-40 of Hamamatsu) and a 610 nm short-pass filter is placed in front of the detector. A 495 long-pass filter separates the blue and the green fluorescence. NADH fluorescence was collected through a 460/480 nm filter. FLIM data is acquired and processed by the SimFCS software developed at the Laboratory of Fluorescence Dynamics. FLIM calibration of the system is performed by measuring the known lifetime of coumarin, with a single exponential of 2.5 ns. FLIM data is collected for over 50 integrated frames. Typically the acquisition time was of the order of few minutes. The laser power was the same for all fields of view.

Data analysis (pCF). Simulations, data acquisition and calculation of the pCF were obtained with custom MatLab code. Simulations can be found in the annexes. The pCF at a given distance in pixels is displayed in an image in pseudocolors in which each colored line represents a certain amount of traveled distance. The x-coordinate is the time and the y-coordinate corresponds to the normalized correlation (Fig. 6C).

Cell sample preparation (SPIM and Laser Scanning Microscopy for N&B). Strips of 2mm x 17 mm were cut from 30 x 24 mm No 1.5 coverslips (Fisher Scientific, Waltham, MA, USA) with a diamond tipped pen. Several of these strips were placed in a 35 mm cell culture dish and coated with of fibronectin (Sigma-Aldrich) prior to plating and transfecting the cells. For fluorescence imaging, single strips were transferred to the imaging dish (Fig. 9). filled with phosphate-buffered saline (PBS).

For the laser scanning microscopy and FLIM, cells were grown in a 35 mm bottom glass cell culture dish, previously coated with 5-$\mu g/cm^2$ fibronectin .

FLIM data analysis. Every pixel of the FLIM image is transformed in one pixel in the 2D histogram of the phasor plot through a fast Fourier transform for the fluorescence intensity[18]. The coordinates g and s (x and y axis of the phasor histogram, respectively) are the real and imaginary part of the FFT. The analysis of the phasor distribution is performed by cluster identification of free and bound NADH. Because of the linearity of the phasor coordinates, mixtures of two components (free and bound NADH) in the focal volume will distribute along the line that connects each component of the two pure components. By using a circular cursor the pixels with the lifetime of interest can be analyzed.

Cell culture. Chinese hamster ovary(CHO-K1) cells stably expressing enhanced green fluorescent protein (EGFP) were cultured in humidified, 5% CO_2 atmosphere at 37^{o}C in Dulbecco's Modified Eagle Medium (DMEM)/Nutrient Mixture F-12(Life Technologies, Rockville, MD) supplemented with 10%fetal bovine serum (FBS), and 0.5 mg/mL geneticin (G418) to maintain selection of transfected cells. Non-transfected CHO-K1 cells were cultured in DMEM/Nutrient Mixture F-12 supplemented with 10% FBS and, 1% (v/v) penicillin/streptomycin.

For fluorescence imaging of Estrogen Receptor Alpha (ERα)-GFP (pEGFP-C1-ER alpha, Addgene), cells were transfected using Lipofectamine 2000 according to the manufacturer's instructions (Life Technologies).

Generally, 1 μg of plasmid (diluted with PBS) was incubated with 5 μl of Lipofectamine for 30 min and added to the cell dish containing fully supplemented media. The cells were maintained in a humidified, 5% CO_2 atmosphere at 37^{o}C and used within 48h. Activation of ERα-GFP was

induced by incubating the cells with medium containing 1 μM 17-β-Estradiol (Sigma-Aldrich) for 10 min.

For Lifetime Imaging of ER-positive breast cancer cells, MCF-7 cells were cultured in humidified, 5% CO_3 atmosphere at 37^{o}C in DMEM-F12 without phenol red, containing 10% charcoal stripped FBS and 1% (v/v) penicillin/streptomycin and the standard tissue culture glucose concentration (450 mg/dl) for "high-glucose" or (100 mg/dl) for "low glucose" for 1 day. Both glucose concentrations are physiological and representative of the *in* vivo differential glucose concentrations in human serum.

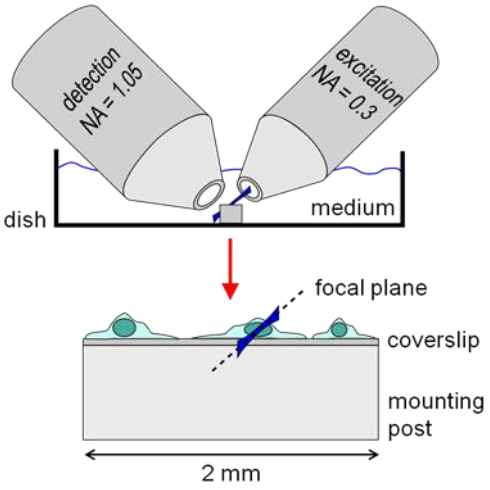

Fig. 9 Schematic of the SPIM setup sample mounting. For cell imaging, a two millimiter wide mounting post is glued to the bottom of a 60 mm tissue culture dish and hold the cells grown on 2mm x 17mm coverslips.

Chapter 4 Results

4.1 From fast imaging to protein dynamics

In this section, the apparent diffusion for the ERα and the GFP is measured by the pCF approach applied to a stack of images obtained through SPIM (section 2). The ligand-specific mobility for these two proteins is observed in the nuclei of living CHO-K1 cells. This is done in order to quantitatively find the mobility as a function of time. Furthermore, it can evaluate how estradiol regulates protein transport and interactions. Fig. 10 Illustrates the analysis method described in section 2.2 in a schematic way. For the stack of images resulting from the fast imaging via single plane illumination microscopy (SPIM)(Fig. 10 A), the pCF at certain radial distance is calculated (Fig. 10 B). If particles diffuse, the width of the correlation increases in time and space.

The correlation as a function of the time at a certain radial distances (r_n) from the initial point can be retrieved (Fig. 10C). Hence, whenever a correlation peak appears the distance from the initial point is known and also the time. Thus, the apparent diffusion over time is retrieved (Fig. 10D)

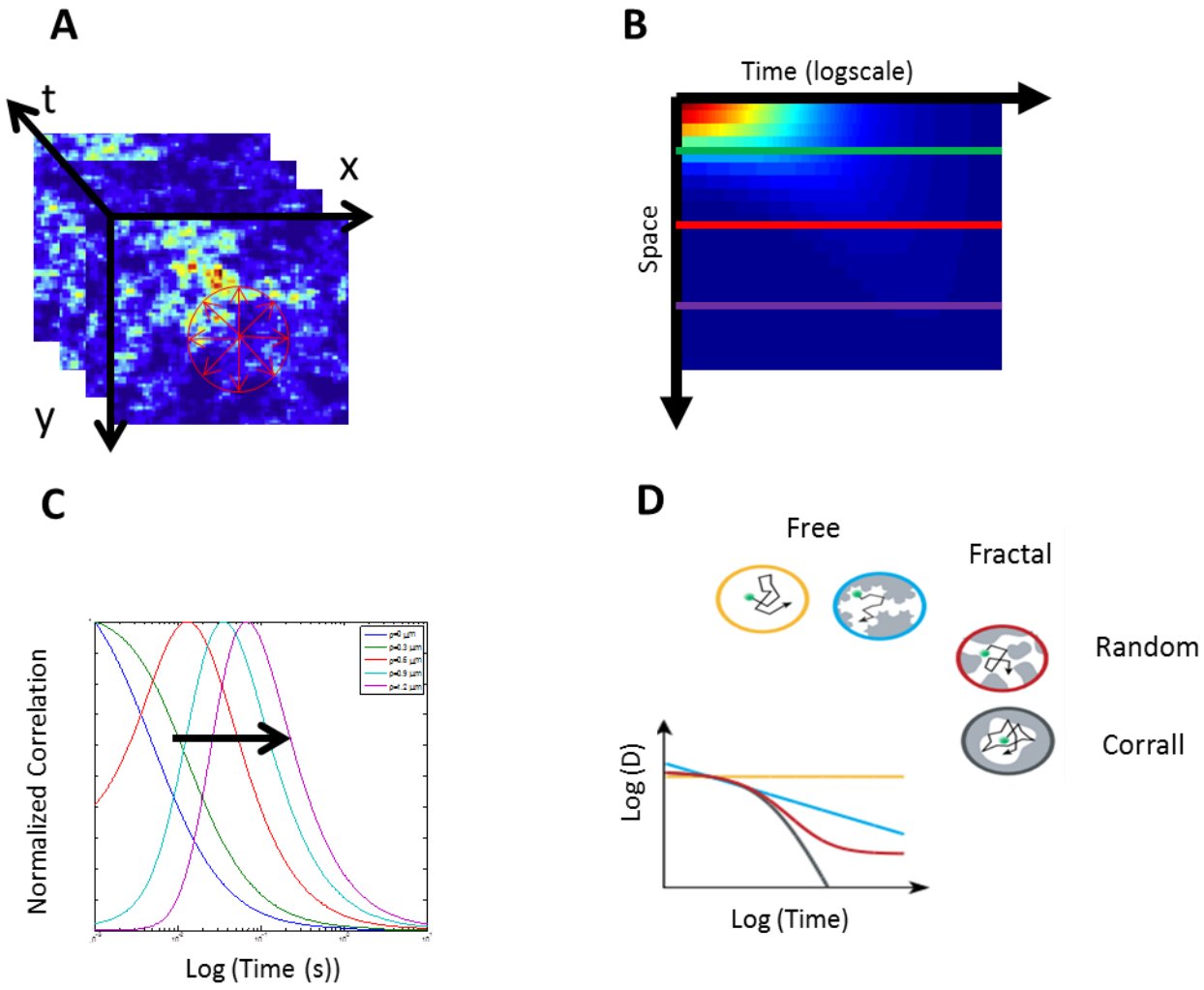

Fig. 10 pCF analysis of the stack of images of live CHO-K1 cell nuclei. (A) From a series of fluorescence images the spatiotemporal correlation is calculated. (B) The data (here, simulated data) are represented in a carpet of pair correlation functions (dark blue= low correlation in space and time, red=high correlation). (C) Normalized pCF as a function of time. Each color represents a certain radial distance from the initial point, fixed by the pixel size (142 nm). (D) The plot of apparent diffusion coefficient as a function of time can be retrieved from the carpet of pCFs. The time dependence of the diffusion coefficient reflects the nano-structural environment that conditions protein movement[16].

4.2 ERα diffusion detection inside Live Cell Nuclei

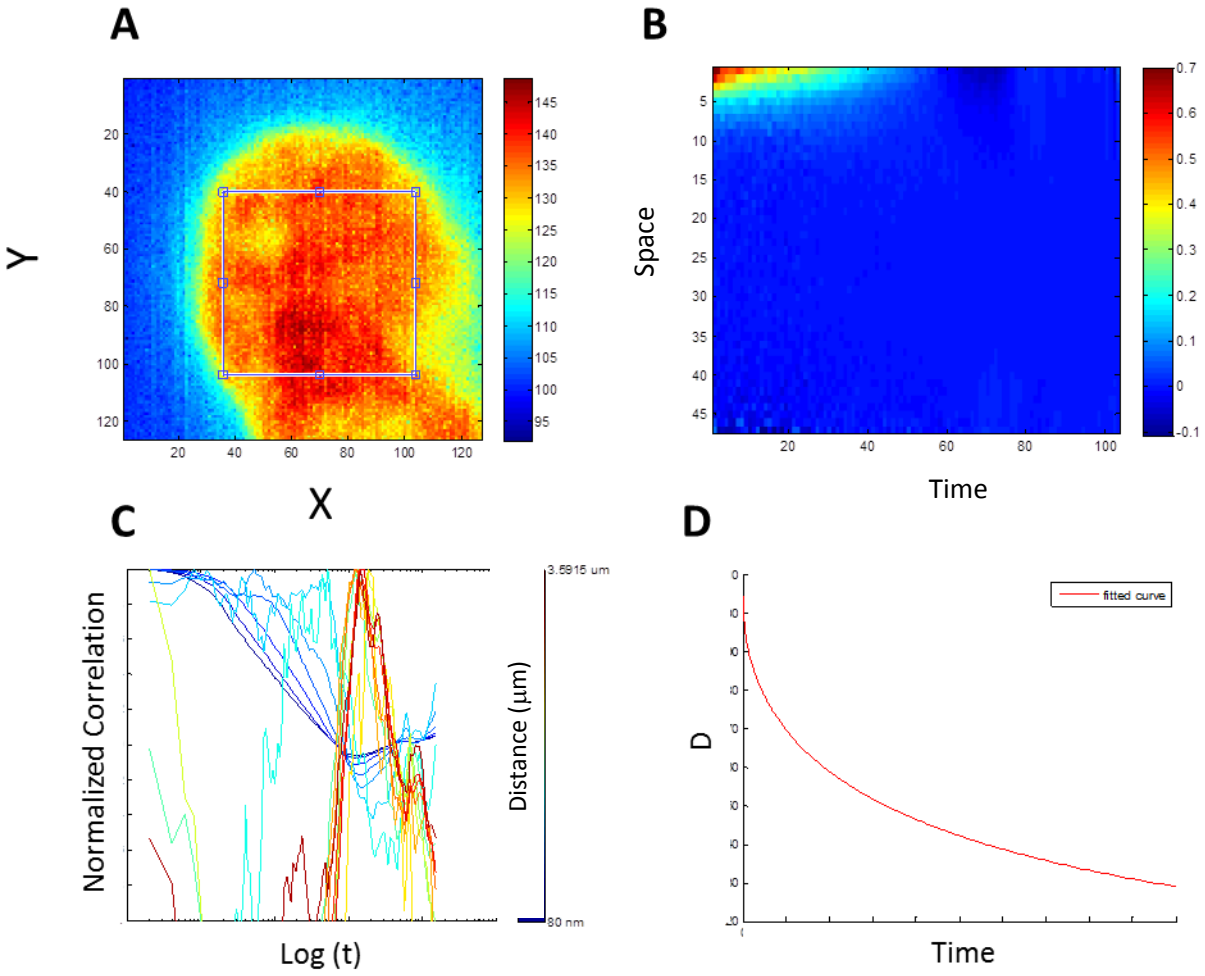

Fig. 11. **pCF analysis in live cell nuclei.** (A)For each cell a region of interest (ROI) is selected for the analysis. (B) As in Fig. 10B, the pCF is calculated at increasing radial distances obtaining the pCF carpet. (C) At every alternate radial distance $(r_1, r_3 \dots r_{n+1})$ from the center of the ROI the correlation is plotted as a function of delay logarithmic time. Each peak can be isolated and analyzed separately to obtain time and distance. (D) Once time and distance are obtained the apparent diffusion $\left(D[\frac{\mu m^2}{s}]\right)$ is calculated and plotted as a function of time.

ERα was chosen as a paradigmatic nuclear transcription factor activated by estrogen. Particularly, a GFP-tagged construct of the ERα was used for transient transfection of live Chinese hamster ovary (CHO-K1) cells. For the analysis a region of between ~200- 500 µm^2 was selected for the analysis (Fig. 11A). The analysis was done over 10,000 frames for each single cell nuclei with a time delay between frames of 2ms (500 frames per second (fps)).

The total acquisition time (~20 s) is long enough to accurately remove the immobile fraction. From the time dependent diffusion coefficient plot $D(t)$ (Fig. 11A, B) and the mean diffusion value (Fig. 13), it can be concluded that the diffusion of the ERα is higher after the addition of 100 nm 17-β-estradiol. Moreover, at short delay times the diffusion for the ERα is higher after the addition of the hormone, but lowers at higher times compared to the unstimulated receptor (Fig. 11A, B).

However, this is not the case for the GFP alone. Either with or without estrogen stimulation the mean diffusion value is not statistically different (Fig. 13). Remarkably, there is a peak increase for the GFP (control) diffusion after stimulation at longer time delay scales (~1-3 seconds).

The data of the mobility for the GFP and ERα-GFG in Fig. 11 was fitted by a simple model for diffusion in porous media consisting of randomly distributed obstacles. The apparent diffusion coefficient is described in the model by the following equation[16]:

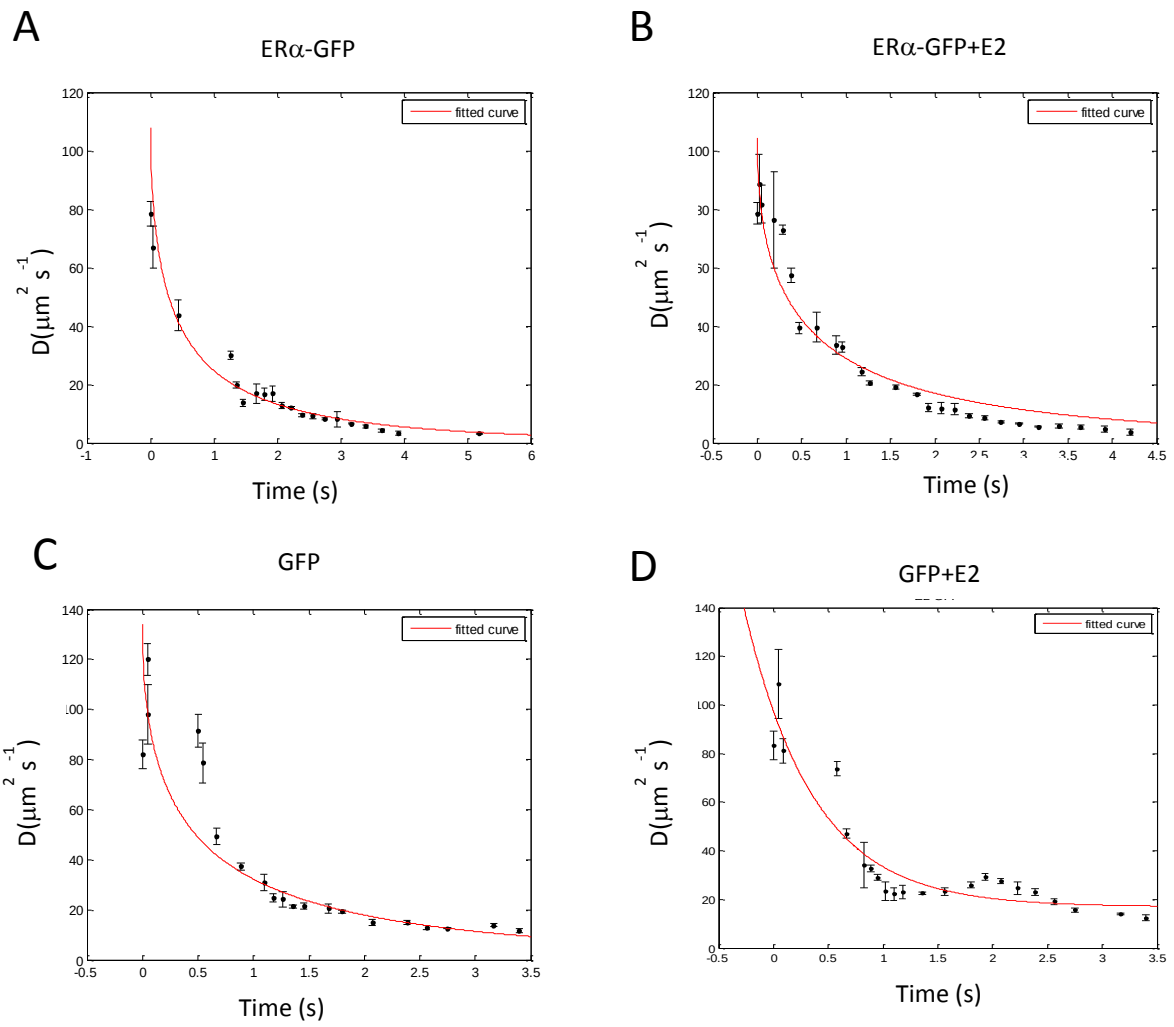

Fig. 12. Time dependence of the diffusion coefficients. Time dependent diffusion coefficients measured in CHO-K1 cells nuclei (A) ERα-GFP time-dependent apparent diffusion coefficient $\boldsymbol{D(t)}$ (n=26 cells). (B) ERα - GFP activated with 100 nM of 17-β-Estradiol time-dependent apparent diffusion coefficient $\boldsymbol{D(t)}$ (n=28cells). (C) GFP alone (control) time-dependent apparent diffusion coefficient $\boldsymbol{D(t)}$ (n=22 cells). (D) GFP alone time-dependent apparent diffusion coefficient $\boldsymbol{D(t)}$ after the addition of 100 nM 17-β-Estradiol (n=23 cells). Continuous lines represent the fitted model given by equation (13)

$$D(t) = (D_0 - D_\infty) \cdot \exp\left(-4\frac{\sqrt{D_0 t}}{\sqrt{\pi\lambda}}\right) + D_\infty \quad (13)$$

This relation contains the following fit parameters: The diffusion for particles at short time/length scale D_0 that describes the mobility without obstacles. The correlation length λ measures the typical distance between obstacles. λ is inversely proportional to the surface-to-volume ratio S/V that the protein encounters during transport. Thus, the importance of the S/V value which characterizes the target search process of the particle, such as finding a binding site in the DNA by a transcription factor. D_∞ is the diffusion coefficient for large time/length scales, in other words, where the MSD grows linearly over time. It is important to note that not all the data points fit properly in this model for this particular study.

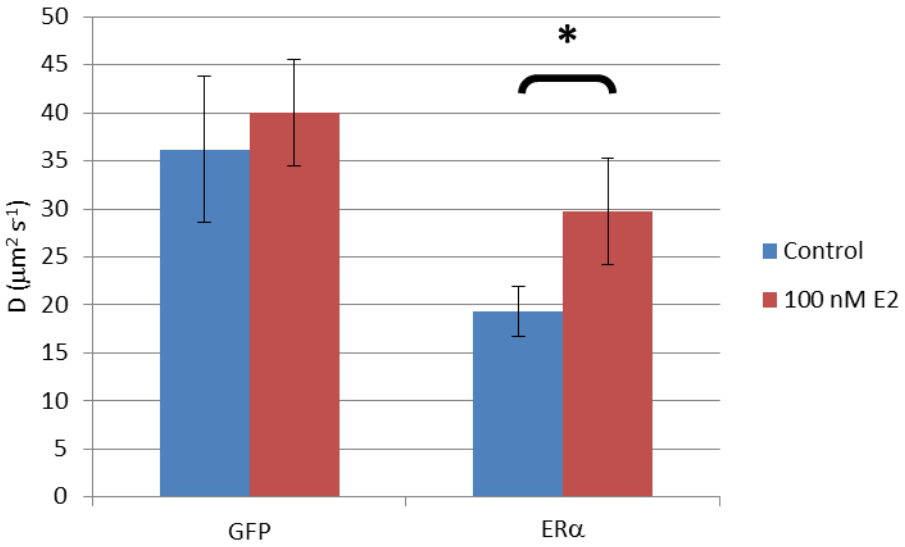

Fig. 13. Mean diffusion values. Estrogen is able to increase the diffusion of the ERα tagged with GFP in the nucleus and that of GFP alone. The difference is only statistically significant for the ERα. *, P < 0.05.

4.3 Retrieving the nuclear topology from binding the map technique.

To expand the information acquired in the previous section, we used the binding map technique (section 2.3). The binding map gives qualitative information of the apparent diffusion of fluorescently labeled proteins. This information is linked to each pixel of an image (Fig. 13.) Therefore, the protein mobility suggests structural features and functional features such as "binding hotspots", barriers or chromatin that regulate movement. The environment that a protein or particle "sees" during its diffusion within a cellular compartment such as the nucleus is plotted (Fig. 14).

The binding map not only retrieves topological and dynamic information about proteins, but also resolves this information at a nano-scale, below the diffraction limit (<140nm). It is straightforward to conclude that there are regions of confinement for the ERα and that there are some regions of "preferred diffusion" for the ERα and some others regions where the transcription factor is more bound to the nuclear structures.

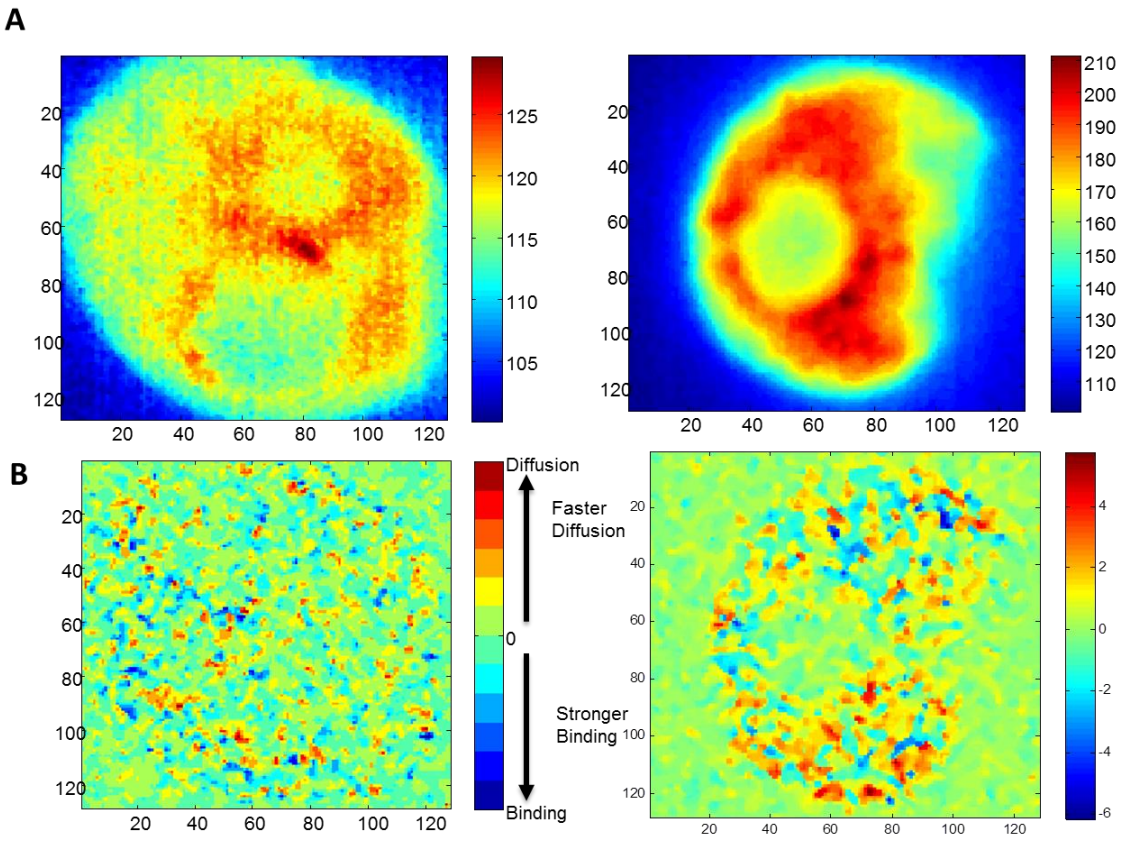

Fig. 14 Binding Map.(A) The left panel is the average intensity map of the ER-eGFP protein in the nucleus. A stack of images is obtained (10,000 frames) with a delay between images of 2ms. On the left panel, another CHO-K1 cell transfected with ERα- GFP plus 100 nM E2. The heat panel on the right shows the average intensity for each cell. (B) For each pixel the "diffusive state" is measured and plotted in a color scale, according to the method explained in section 2.3. The higher the diffuse slope ($\boldsymbol{\theta_D}$) the warmer the color. The higher the absolute value of the binding slope ($\boldsymbol{\theta_B}$) the cooler the color. Notably, not all regions show diffusion or binding suggesting barriers or "binding and diffusion hotspots"

4.4 ERα concentration-dependent localization

ERα is a key regulator of cell homeostasis and fate. It is a highly localized protein that can be found in different cellular regions (e.g. Nucleus, cytoplasm, mitochondria). It is well documented that depending on this subcellular localization a range of different functions are carried out (e.g from fast-signaling to gene transcription). Remarkably, the ERα is frequently overexpressed in the early stages of breast cancer[2].

Mammalian cells are highly compartmentalized and generally, most proteins show a localization pattern in the cell. Generally, this localization is due to the specific function of the particular protein. Thus, the same protein can carry out different functions depending on its localization. The N&B method, as explained in detail in section 2.5, helps us retrieve the average number of molecules in an image.

CHO-K1 cells transiently transfected with ER were analyzed in order to understand the distribution of the transcription factor (

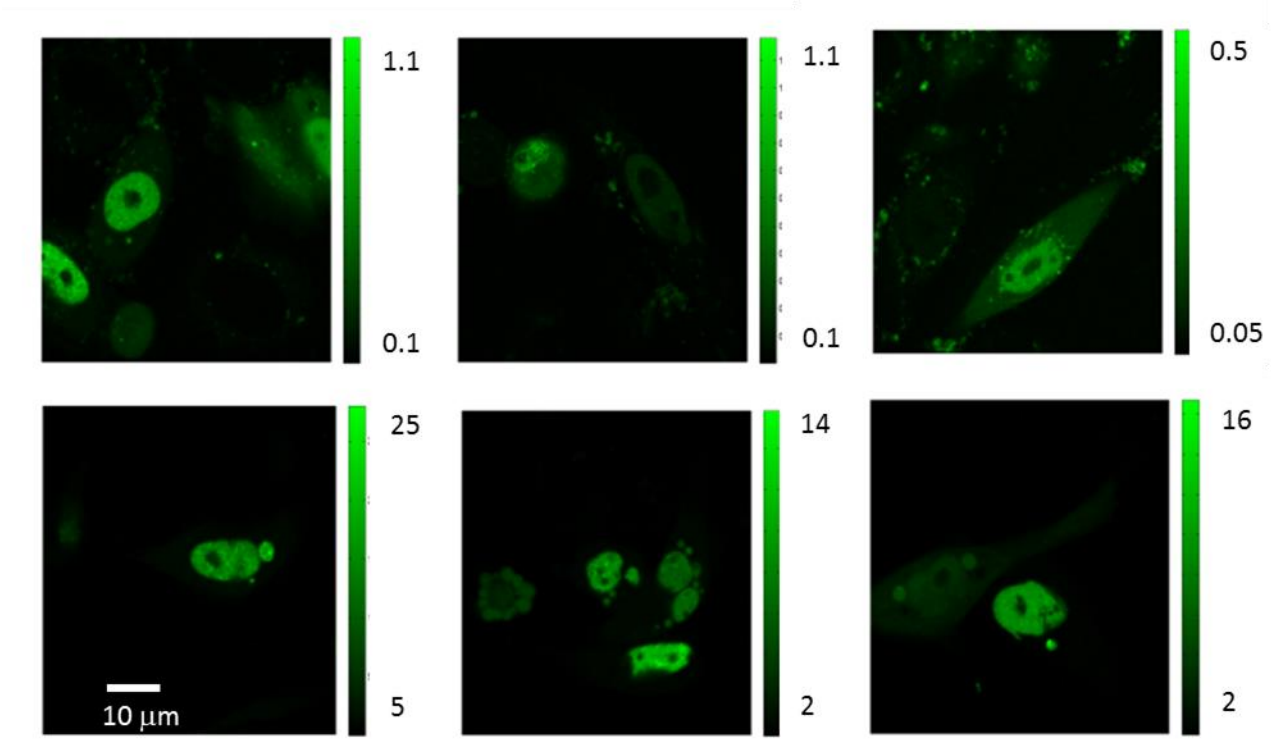

Fig. 15). Each analyzed cell was analyzed in 3 different regions: Nuclear, cytoplasmic and membrane region (~1μm) by manually selecting the regions with custom-made MatLab code (Fig. 16). For each of these regions, the average, the median and the maximum ERα concentration was quantified. All these quantities are then normalized by the average ERα concentration (i.e. a maximum ER α concentration of 10 A.U. in the nucleus indicates that the brightest pixel in the nucleus has a fluorescence intensity that is 10 times higher than the average cell fluorescence).

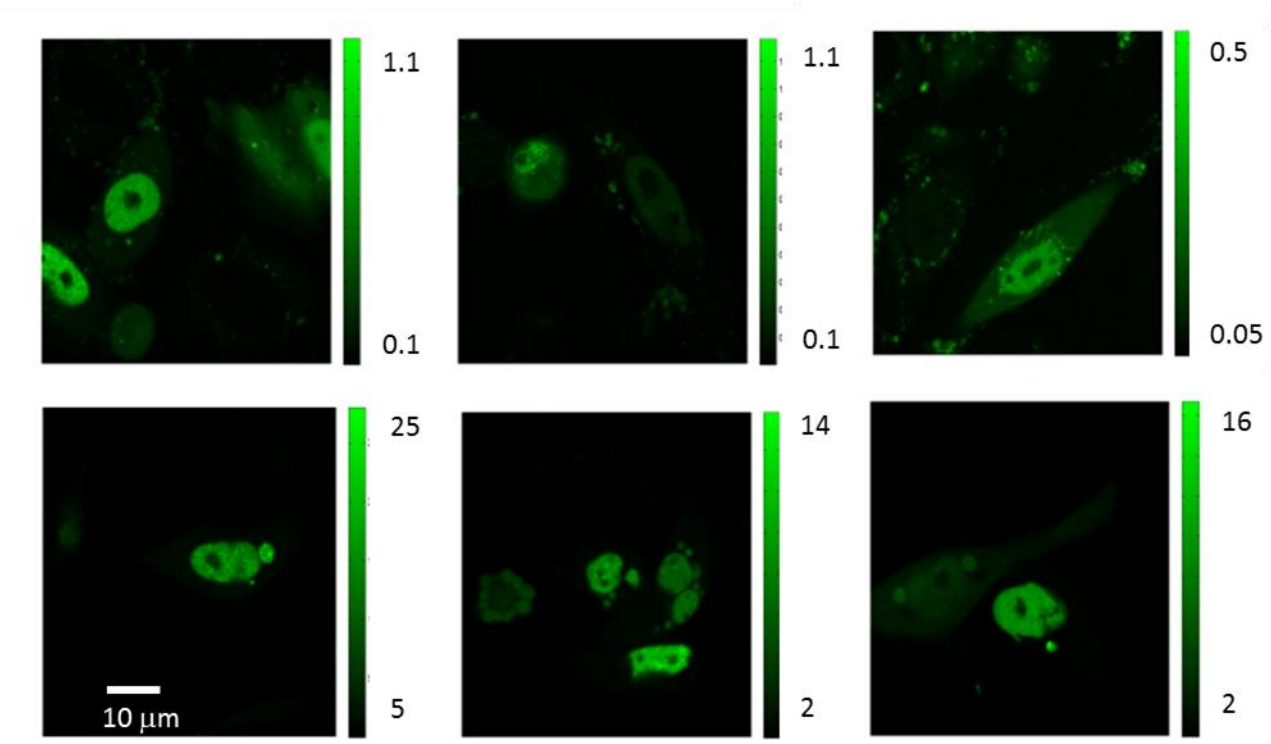

Fig. 15. ERα in CHO-K1 cells. Fluorescence intensity images of cells expressing ERα-GFP obtained with laser scanning microscopy. Depending on the expression levels/concentration of the protein its subcellular location changes. ERα is mostly located in the nucleus in the top left panel whereas in top right panel it can be detected in the cytoplasmic region too. Intensity is in arbitrary units (A.U.)

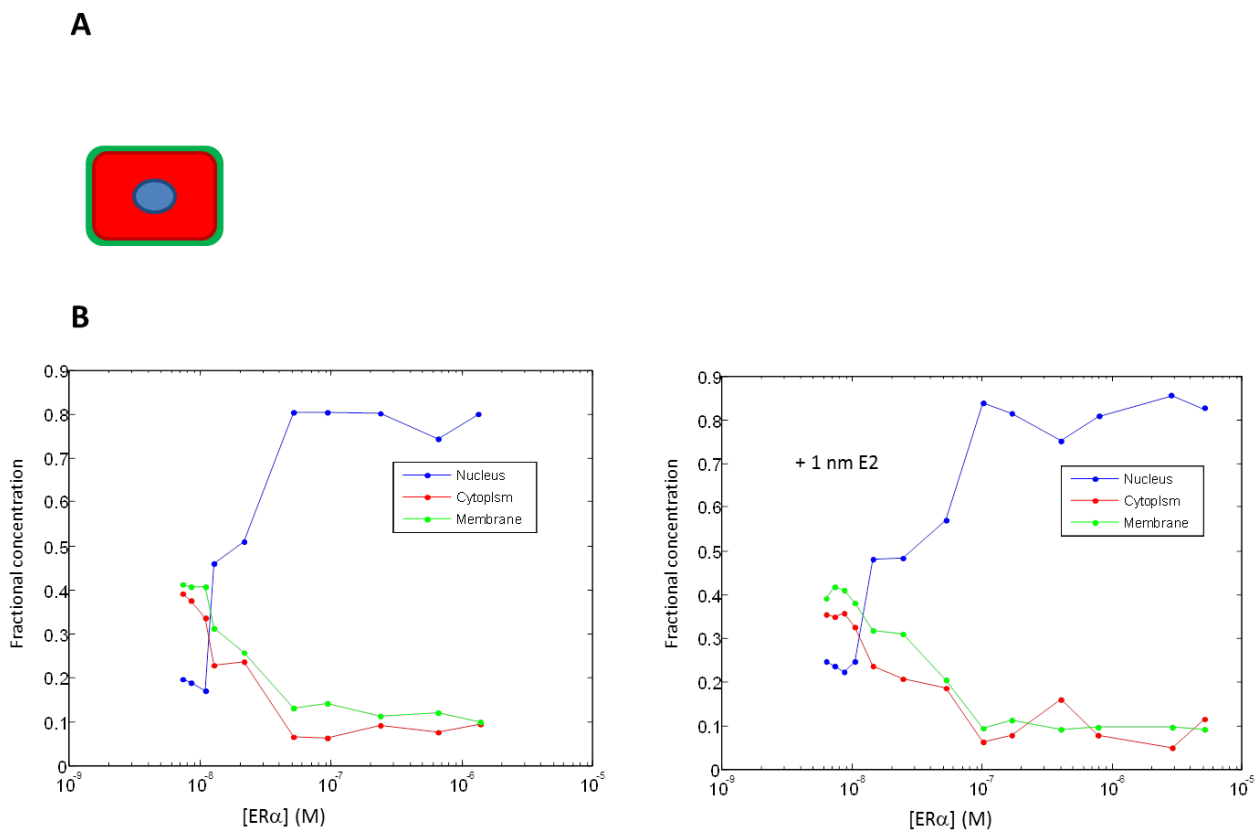

Fig. 16. ERα subcellular localization as a function of concentration. (A) Schematically, three regions for each cell were analyzed separately in order to obtain concentrations for the ERα. Nucleus (blue), cytoplasm (red) and membrane (green) (B) Fractional concentration of ERα in each of the three subcellular compartments analyzed as a function of total ERα concentration without E2 stimulation (left, n= 83 cells) or with 1nM of E2 (right, n=104 cells)

Traditionally the distribution for the ERα is believed to be as follows: ~85% of the total amount is located in the nucleus, 10% between cytoplasm and mitochondria and 5 % at the plasma membrane[7]. However, it is safe to argue that at low receptor concentrations (~10nM) the aforementioned percentages change (Fig. 16, top). Notably, at higher ERα concentrations (~1μm) most of the receptor (~90% of the total amount) is localized inside the nucleus (Fig. 16B, bottom).

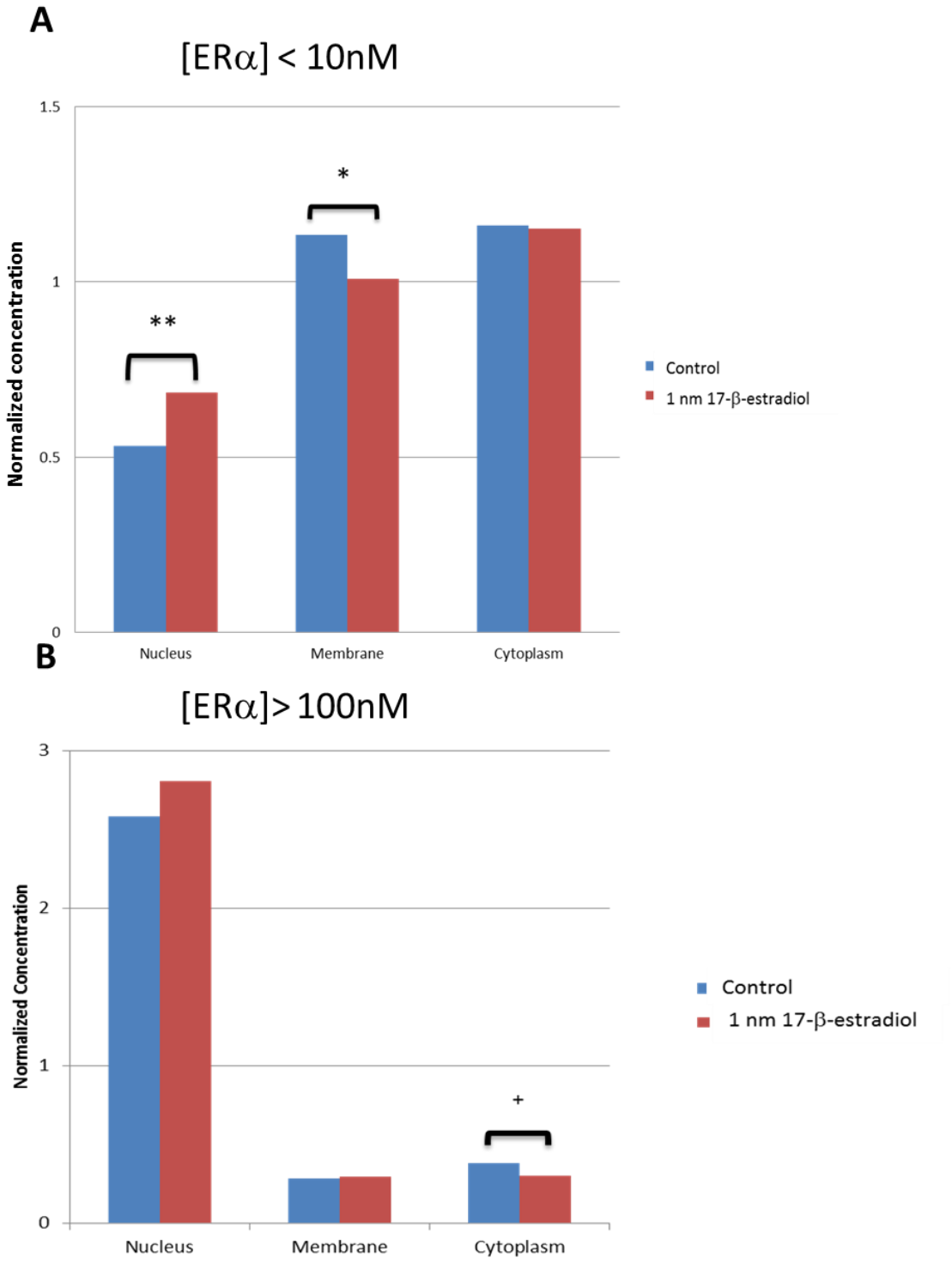

Fig. 17 ERα concentration in different subcellular compartments. Two different ERα concentration ranges are studied:(A) ERα concentrations that are <10 nM (n= 300 cells). (B) ERα concentrations that are >100 nM. *, P<0.05.**, P<10^{-6}. .+, P<0.05. Normalization is done by dividing by the average concentration in the cell (n=296 cells).

Different estradiol concentrations were tested in order to assess if they affected ERα localization. Moreover, different concentrations of the estradiol could have different effects depending on the overall concentration of ERα. At low receptor concentrations, the localization is mainly cytoplasmic and in the cellular membrane (Fig. 17A). After activation with 1nM of E2, the pool in the membrane is reduced whereas the nuclear pool increases. This could suggest transport between these two compartments due to hormonal activation (Fig. 17A). On the other hand, at receptor concentrations higher than 100 nM, the receptor is mostly localized in the nucleus. Furthermore, after hormonal activation the cytoplasmic pool diminishes and the nuclear increases even more. This suggests that at high receptor concentrations the transport could be between the cytoplasm and the nucleus, in contrast to the results found at lower receptor concentrations (<10 nM ERα/cell)(Fig. 17 A, B).

Finally, there is a relationship between the receptor concentration and the concentration of hormone needed to trigger the change in localization for the ERα. At lower receptor concentrations (~10 nM), close to the described physiological range (~1-5 nM), the necessary amount of E2 to increase the ERα nuclear population is 10 times higher (~1nM) (Fig. 18A). On the other hand, at higher ERα concentrations (>100 nM), 10 times less hormone is needed for increased nuclear ERα level compared to other subcellular compartments (i.e. Membrane and cytoplasm)(Fig. 18B).

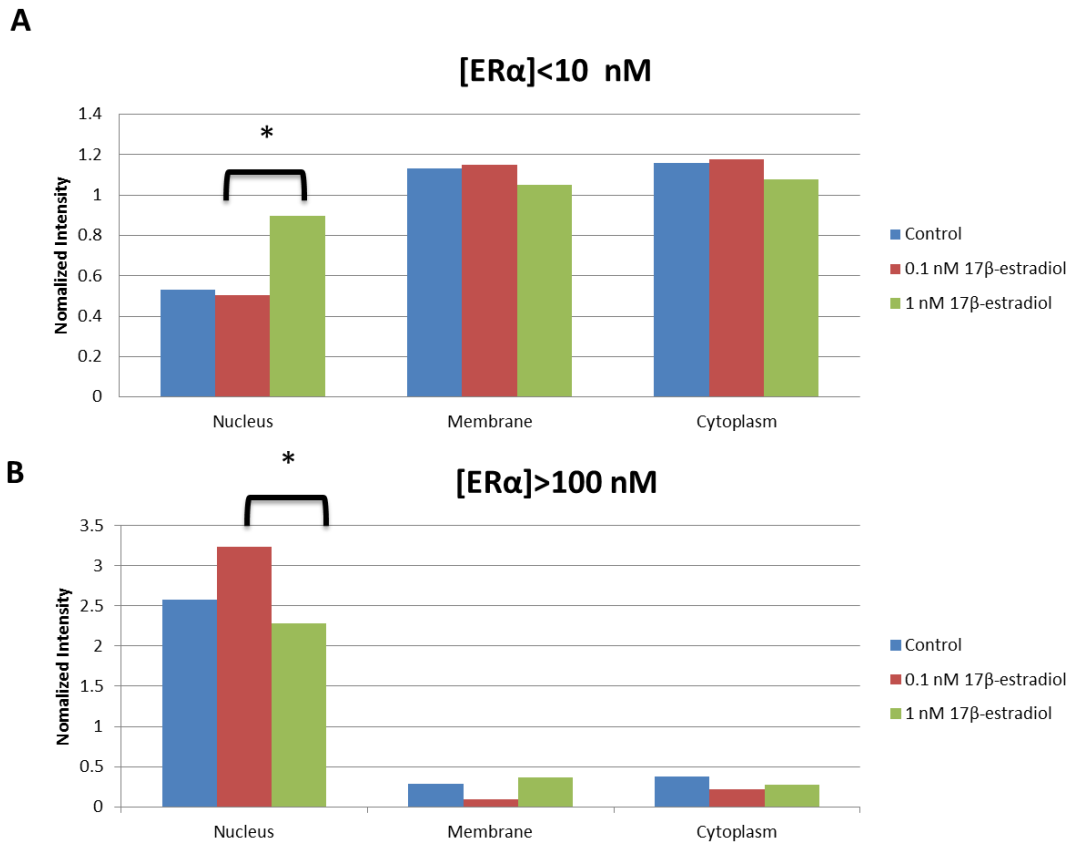

Fig. 18 Effect of different hormone concentrations in terms of activation and subcellular localization. CHO-K1 cells transiently transfected with ERα-GFP**.** Three conditions are tested: Absence of hormone (control), 0.1 nM E2 and 1 nM E2. (A) ERα concentrations <10 nM. (B) ERα concentrations >100 nm. Three conditions are tested: Absence of hormone (control), 0.1 nM E2 and 1 nM E2. *, P<0.05.

4.5 In vivo single-cell detection of metabolic pathways in breast cancer cells

In cancer biology, it is generally accepted that cancer cells use glucose as a substrate in order to perform aerobic glycolysis over oxidative phosphorylation. However, cancer cells have the capacity to adapt to variable glucose concentrations that arise in in-vivo tumors. Furthermore, it has been reported that the estrogen receptors play a role in modulating these metabolic adaptations. Specifically, MCF-7 cells (ERα-positive, breast cancer) switch between metabolic pathways as a function of the glucose availability and E2 presence[20].

Here we present an imaging based analysis method that allows for the measurement of the fluorescence decay from different molecular species within the cell. Fluorescence lifetime imaging microscopy (FLIM), together with the phasor approach, allows for a simple analysis for the fluorescence decay occurring at each pixel of an image, as thoroughly explained in section 2.4[17].

This is a sensitive, non-invasive approach to detect the free and bound ratios of reduced nicotinamide adenine dinucleotide (NADH). This is indicative of the glycolysis/oxidative phosphorylation ratio of cells[19]. *In vivo* imaging of NADH autofluorescence by excitation at 740nm within MCF-7 cells was performed. 4 conditions were tested: High glucose (~450mg/dl), low glucose (~100 mg/dl), addition of 1nM E2, no hormonal stimulation (control) (Fig. 19).

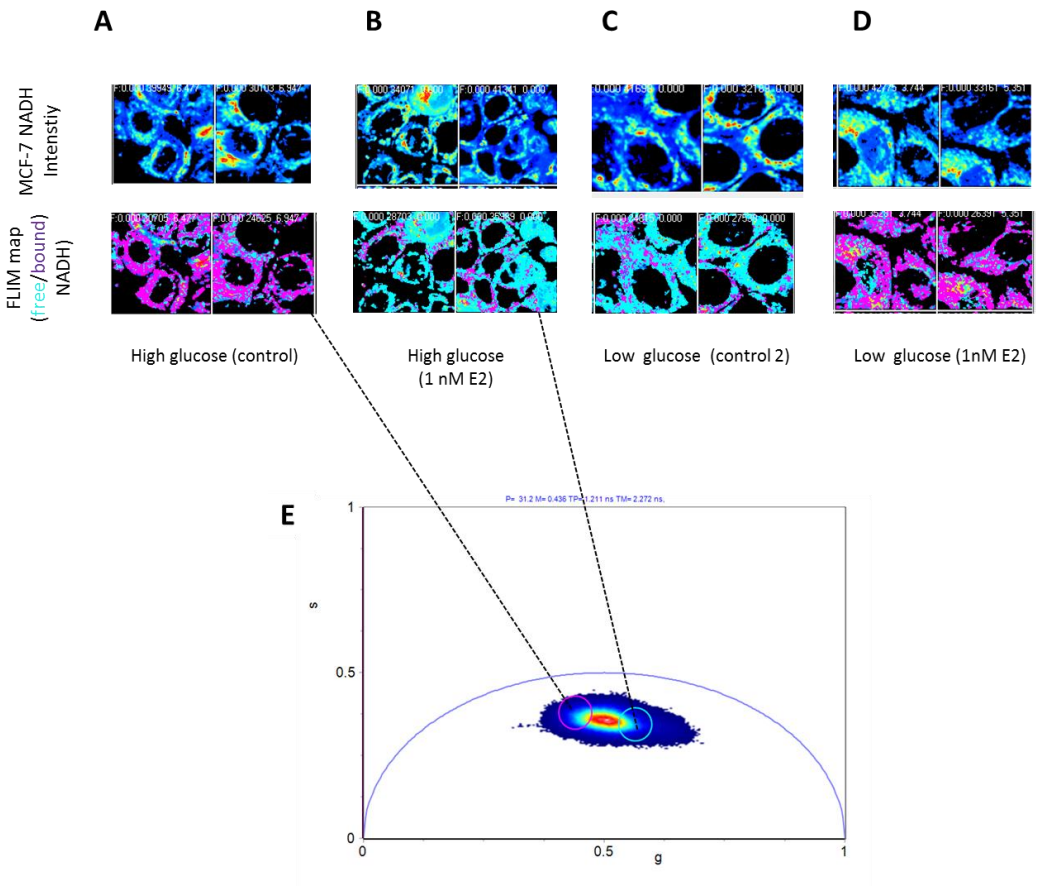

Fig. 19. Metabolic plasticity in MCF-7 breast cancer cell lines. In vivo intensity images of MCF-7 cells after excitation at 740 nm by a femtosecond laser and FLIM color maps for the relative presence of free and bound NADH. Purple color a decreasing free/bound NADH ratio, whereas cyan color indicates a high free/bound NADH ratio.(A) Cells were cultured at high glucose (~450 mg/dl) and no estrogen stimulation (n=59 cells). (B) Cells were cultured at high glucose and 1nm E2 (n=50 cells). (C) Cells cultured at low glucose (100 mg/dl) without estrogen addition (n=45 cells). (D) Cell were cultured at low glucose and 1nm E2 (n=53 cells). (E) Phasor approach for the analysis of FLIM images, performed both at the pixel level and cell level. Single pixels are painted in the FLIM map according to the color of the Violet and Cyan cursors that corresponds to different ratios of free and bound NADH. Pixels within the lifetime coordinates $(\boldsymbol{g}, \boldsymbol{s})$ of each cursor are painted in the FLIM map according to the color of the respective cursor.

Two-photon fluorescence intensity for NADH distribution within the cell highlights the morphology of single cells with relatively dim nuclei and bright mitochondria (Fig. 19A, B, C, D). The analysis of the FLIM images is performed by a fast Fourier transform (FFT) of the FLIM raw data by creating a 2D histogram (phasor plot) of the NADH FLIM image where every pixel of the FLIM image is transformed into a pixel in the phasor plot[19] (Fig. 19E, Fig. 20).

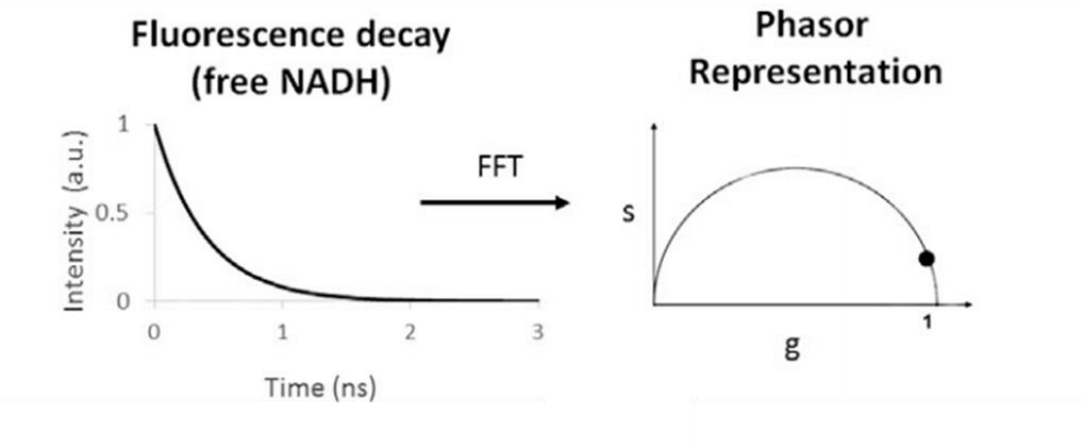

Fig. 20 Illustrative representation for the mathematical transformation of fluorescence decay raw data. By using a fast Fourier transform (FFT)[17], the measure lifetime decay is represented in a 2D phasor plot with g and s coordinates corresponding to the real and imaginary part of the FFT. The phasor coordinates are linear. Thus, mixtures of two components such as free and bound NADH in the focal volume under study will lay along the pure molecular species[18]

It is observed that at high glucose, without E2 addition, the cells and at low glucose, plus 1nM E2, present a higher amount of bound NADH, which is associated with a higher amount of oxidative phosphorylation (Fig. 19 A, D). On the contrary, cells cultured at either high glucose levels and estradiol or low glucose without estradiol show a higher amount of free NADH. Generally, this is characteristic fingerprint of glycolysis[18,19].

Chapter 5 Discussion

5.1 pCF and Binding Map

In this study we proposed an image-correlation analysis method for the *in* vivo study of protein dynamics inside the nuclei. This method has the same mathematical basis of the pair correlation function (pCF)[27,28]. However, the temporal resolution in the present study is brought down to the millisecond (ms) range. By doing that, we are able to capture not only slow but also fast diffusive dynamics as well. Furthermore, the analysis of the complete space-time correlation function, the temporal evolution of the diffusive behavior for proteins inside the nucleus can be monitored. However, it is important to note that this approach does no track every particle separately. Instead, the population behavior inside the ROI is probed as an average. In the case of pure diffusion of the proteins, the correlation is broadened in space and time (Fig. 21A). If proteins are bound the correlation is narrow in space (Fig. 21B). Finally, for a mixture of binding and diffusion the correlation is also a mixture (Fig. 21C). By studying the correlation at periodically fixed radial distances over time the diffusion as a function of time plot is obtained. Compared to other methods such as fluorescence correlation spectroscopy (FCS), the Diffusion vs. time plot can be easily reconstructed on a wide array of spatial and temporal scales[29–31]. Moreover, the description obtained is quantitative and describes the temporal evolution of the diffusion from the average molecular positions with a submicron accuracy.

By using a GFP tagged version of the ERα the regulation of protein diffusion by nuclei structures

was tracked. Remarkably, we obtain values for the mean diffusion of the ERα-GFP and GFP alone. By fitting to a model we are also able to obtain the diffusion values for short time scales (~80 $\mu m^2/s$) for both proteins. Moreover, the diffusion of the particle at long time scales is also retrieved in the nucleus of live CHO-K1 cells (~5 $\mu m^2/s$ for the ERα and ~20 $\mu m^2/s$ for GFP alone). This is in good agreement with previous reported measurments[15,16,10]. The lower diffusion coefficient for the ERα could be arguably due to the binding of the protein to its specific DNA target sites and/or because the receptor dimerizes (this is further increased by the addition of hormone[1,114,16]), increasing the particle size and making the movement around a meshwork of obstacles more difficult. However, the brightness of the particles was not measured.

Therefore, this approach not only retrieves information in a scale-dependent manner, but also provides structural information on the nanometer scale. Diffusion barriers were observed through both the pCF and the binding map inside the nucleus. Hence, this method extends the available repertoire of analysis techniques to study changes in molecular transport.

It can be anticipated that the size-dependent difference between particles (monomer vs. dimer) can have a large impact on the target search mechanism, which results in cellular functions later on. Finally, the unveiled information regarding diffusion and binding with the pCF and the binding map might have a functional link between the chromatin architecture, protein transport and gene transcription. This can be relevant to the clinical impact of the ERα, in breast cancer, in addition to the already established modes of action. SPIM microscopy allows for plane optical sectioning. This together with a suitable analysis to retrieve internal

cellular organization that governs mobility, binding and other interaction of proteins in live cells can provide a new insight into the interaction between function and structure.

Ultimately, these interactions can help us to better understand the pathology of certain diseases such as breast cancer.

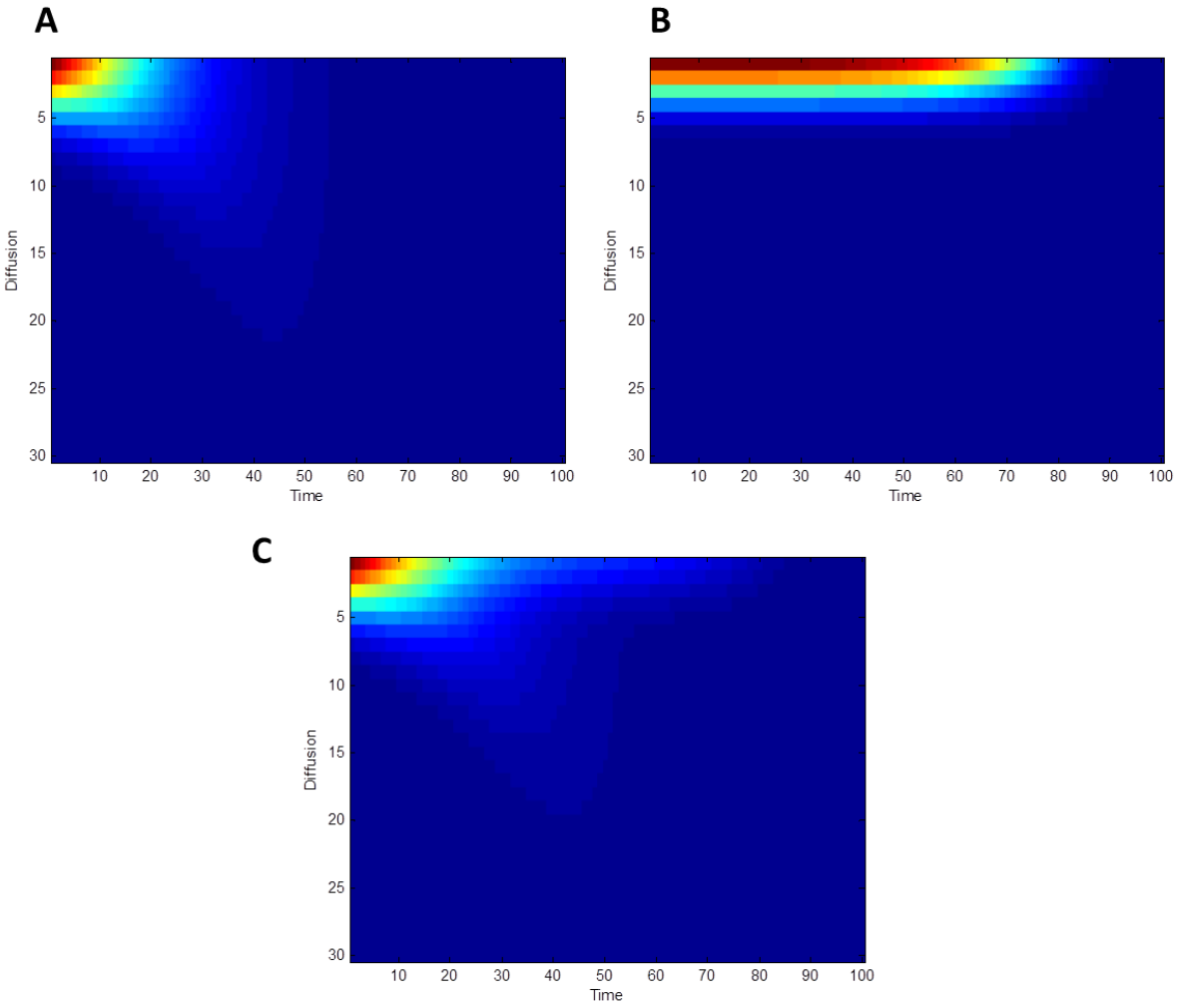

Fig. 21 Simulated correlation functions. (A) Correlation function for pure diffusion of particles according to equation . (B) Correlation function for pure binding of particles. (C) Correlation function for a mixture of diffusion and binding.

5.2 N&B

A particular protein function not only depends on its dynamics in terms of apparent diffusion, but also on its micro-environment. It can be anticipated that in different cellular compartments, a protein may have a different set of interactions with other proteins, substrates, obstacles, barriers, cytoskeleton and so on.

The N&B analysis provides further insight in that regard by measuring the apparent brightness and number of molecules in every pixel of an image, as already discussed previously. While in the previous section the spatiotemporal fluctuations can be measured for particles, the N&B analysis exploits fluorescence amplitude fluctuations to provide information regarding particle localization, brightness and number[32]. Notably, the results suggest that the required amount of hormone is dependent on the amount of available receptor (Fig. 18). Moreover, depending on the concentration ERα, after activation the increase in the nuclear pool might come from different cellular pools other than the nucleus itself. Thus, at low receptor concentrations, after activation with E2 the membrane pool is reduced in order to increase the nuclear pool, whereas at high receptor concentration the cytoplasmic pool is the one that mobilizes into the nucleus. Finally, it is evident from the results (Fig. 18) that the distribution for cellular receptors within different cellular regions might be very different from what is classically thought to be, as the levels of expression vary.

5.3 FLIM

Previous studies have shown breast cancer cell metabolic plasticity by traditional biochemical analysis[20,33].Moreover, estrogen receptors potentiates this adaptation in the presence of E2[20].In this study we provide a single cell resolution, label free technique that is able to distinguish between free NADH and NADH bound to proteins *in vivo* and *in vitro*[19]. It can be argued that these two different populations are characteristic features of glycolysis and oxidative phosphorylation, respectively. The implementation of FLIM overcomes some of the problems of other traditional techniques required to perform these studies, allowing detection of metabolic states of MCF-7 cells just by imaging.

Notably, the results oppose the original Warburg hypothesis that suggests that cancer cells have dysfunctional mitochondria, being unable to undergo oxidative phosphorylation. This is in good agreement with previous studies[20,34,35] . Furthermore, due to the complexity of tumor biology, different areas within a tumor may have differential oxygenation levels and glucose concentrations[20,36]. Due to varying conditions cells may adapt to the conditions imposed by the specific environment, by altering the metabolic pathways in order to proliferate efficiently. However, not only the particular glucose availability but also other cell signaling factors, such as E2/ER presence, like in this particular study, may promote these changes to enhance survival of neoplasic tissue.

Finally, the findings suggest that FLIM can be a useful tool in order to quickly and reliably asses metabolic states and metabolic plasticity. Understanding cancer cell adaptations

to different environmental conditions can lead to novel clinical and therapeutic approaches in order to better suppress tumor progression.

Chapter 6 Conclusions and future directions

6.1 Conclusions

The combination of different biophysical techniques such as the pCF, the binding map, N&B and FLIM can help us retrieve valuable information about proteins. The scale-dependent mobility of nuclear factors such as the ERα obtained by STICS sheds light on the intracellular architecture and the binding properties of these proteins. Moreover, by using N&B the localization of the protein can be known together with the state of oligomerization of the protein (Note that brightness was not measured in this study). Finally, functional information can be retrieved directly by applying FLIM and the phasor approach. It can be anticipated that the integration of these analysis techniques might complement the reported information about transcriptions factors, specifically in disease-related deregulation. Thus, a biophysical arsenal of analytical tools is ready to be tested in dedicated experiments that are beyond the scope of the present study. Hopefully, the synthesis of these techniques, together with other types of approaches, can identify the basic principles that rule in disease in order to better tackle it.

6.2 Future directions

For the pCF analysis longer length/ time scales should be studied. This is because as proteins diffuse, diffusion barriers are found in both the nucleus and the cytosol, changing the behavior of the apparent diffusion. Some controls might be needed such as performing the analysis for suitably tagged non-mobile proteins (i.e. Histones), perturbing the chromatin structure as a control in order to test the chromatin role as a "barrier" for protein diffusion. Furthermore, the model used to fit the data in Eq. (13) does fit all the points in all the experimental conditions. Hence, developing a proper model can unveil additional and more suitable information map intracellular structure. In addition, the binding map is a technique still in an early development stage. It is highly computational demanding so improvements can be made on the code to generate maps faster, among others.

Regarding the N&B analysis, further testing in other cell lines, different proteins of interest and higher range of particle concentrations is needed. The localization as a function of concentration might be cell type dependent too. Moreover, studying oligomerization through the brightness part of the technique will reveal the localization and the number of molecules that aggregate under certain conditions, in live cells.

Finally, for the FLIM analysis quantitative results are needed for this particular study together with the analysis of other ER-positive cell lines under a broader range of conditions.

BIBLIOGRAPHY

1. Heldring, N. *et al.* Estrogen Receptors : How Do They Signal and What Are Their Targets. 905–931 (2007). doi:10.1152/physrev.00026.2006.

2. Hayashi, S.-I. *et al.* The expression and function of estrogen receptor alpha and beta in human breast cancer and its clinical application. *Endocr. Relat. Cancer* **10,** 193–202 (2003).

3. Heldring, N., Nilsson, M., Buehrer, B., Treuter, E. & Gustafsson, J.-A. Identification of tamoxifen-induced coregulator interaction surfaces within the ligand-binding domain of estrogen receptors. *Mol. Cell. Biol.* **24,** 3445–3459 (2004).

4. Nilsson, S. *et al.* Mechanisms of estrogen action. *Physiol. Rev.* **81,** 1535–1565 (2001).

5. Dutertre, M. & Smith, C. L. Molecular mechanisms of selective estrogen receptor modulator (SERM) action. *J. Pharmacol. Exp. Ther.* **295,** 431–437 (2000).

6. Goodsell, D. September 2003 Molecule of the Month - Estrogen Receptor. *RCSB Protein Data Bank* (2003). at <http://www.rcsb.org/pdb/101/motm.do?momID=45>

7. Levin, E. R. Minireview: Extranuclear steroid receptors: roles in modulation of cell functions. *Mol. Endocrinol.* **25,** 377–384 (2011).

8. Htun, H., Holth, L. T., Walker, D., Davie, J. R. & Hager, G. L. Direct visualization of the human estrogen receptor alpha reveals a role for ligand in the nuclear distribution of the receptor. *Mol. Biol. Cell* **10,** 471–86 (1999).

9. Deroo, B. & Korach, K. Estrogen receptors and human disease. *J. Clin. Invest.* **116,** 561–570 (2006).

10. Jankevics, H. *et al.* Diffusion-time distribution analysis reveals characteristic ligand-dependent interaction patterns of nuclear receptors in living cells. *Biochemistry* **44,** 11676–11683 (2005).

11. Digman, M. A. & Gratton, E. Imaging barriers to diffusion by pair correlation functions. *Biophys. J.* **97,** 665–673 (2009).

12. Axelrod, D., Koppel, D. E., Schlessinger, J., Elson, E. & Webb, W. W. Mobility measurement by analysis of fluorescence photobleaching recovery kinetics. *Biophys. J.* **16,** 1055–1069 (1976).

13. Chen, H., Farkas, E. R. & Webb, W. W. Chapter 1 In Vivo Applications of Fluorescence Correlation Spectroscopy. *Methods in Cell Biology* **89,** 3–35 (2008).

14. Di Rienzo, C., Gratton, E., Beltram, F. & Cardarelli, F. Fast spatiotemporal correlation spectroscopy to determine protein lateral diffusion laws in live cell membranes. *Proc. Natl. Acad. Sci. U. S. A.* **110,** 12307–12 (2013).

15. Hedde, P. N., Stakic, M. & Gratton, E. Rapid Measurement of Molecular Transport and Interaction inside Living Cells Using Single Plane Illumination. *Sci. Rep.* **4,** 7048 (2014).

16. Baum, M., Erdel, F., Wachsmuth, M. & Rippe, K. Retrieving the intracellular topology from multi-scale protein mobility mapping in living cells. *Nat. Commun.* **5,** 4494 (2014).

17. Digman, M. a, Caiolfa, V. R., Zamai, M. & Gratton, E. The phasor approach to fluorescence lifetime imaging analysis. *Biophys. J.* **94,** L14–L16 (2008).

18. Stringari, C. *et al.* Phasor approach to fluorescence lifetime microscopy distinguishes different metabolic states of germ cells in a live tissue. *Proc. Natl. Acad. Sci. U. S. A.* **108,** 13582–13587 (2011).

19. Stringari, C. *et al.* In Vivo Single-Cell Detection of Metabolic Oscillations in Stem Cells. *Cell Rep.* **10,** 1–7 (2015).

20. O'Mahony, F., Razandi, M., Pedram, A., Harvey, B. J. & Levin, E. R. Estrogen modulates metabolic pathway adaptation to available glucose in breast cancer cells. *Mol. Endocrinol.* **26,** 2058–70 (2012).

21. Magde, D., Elson, E. & Webb, W. W. Thermodynamic fluctuations in a reacting system measurement by fluorescence correlation spectroscopy. *Phys. Rev. Lett.* **29,** 705–708 (1972).

22. Höfling, F. & Franosch, T. Anomalous transport in the crowded world of biological cells. *arXiv* 1–55 (2013). doi:10.1088/0034-4885/76/4/046602

23. Digman, M. a, Stakic, M. & Gratton, E. *Raster image correlation spectroscopy and number and brightness analysis. Methods in enzymology* **518,** (Elsevier Inc., 2013).

24. Otto, C. *et al.* G protein-coupled receptor 30 localizes to the endoplasmic reticulum and is not activated by estradiol. *Endocrinology* **149,** 4846–4856 (2008).

25. Gratton, E. The Number & Molecular Brightness (N & B) Method.

26. RYAN A. COLYER, CLAUDIA LEE, A. E. G. A Novel Fluorescence Lifetime Imaging System ThatOptimizes Photon Efficiency. *Microsc. Res. Tech.* **71,** 201–213 (2008).

27. Hebert, B., Costantino, S. & Wiseman, P. W. Spatiotemporal image correlation spectroscopy (STICS) theory, verification, and application to protein velocity mapping in living CHO cells. *Biophys. J.* **88,** 3601–3614 (2005).

28. Cardarelli, F. & Gratton, E. In vivo imaging of single-molecule translocation through nuclear pore complexes by pair correlation functions. *PLoS One* **5,** (2010).

29. Wawrezinieck, L., Rigneault, H., Marguet, D. & Lenne, P.-F. Fluorescence correlation spectroscopy diffusion laws to probe the submicron cell membrane organization. *Biophys. J.* **89,** 4029–4042 (2005).

30. Ruprecht, V., Wieser, S., Marguet, D. & Schütz, G. J. Spot variation fluorescence correlation spectroscopy allows for superresolution chronoscopy of confinement times in membranes. *Biophys. J.* **100,** 2839–2845 (2011).

31. Eggeling, C. *et al.* Direct observation of the nanoscale dynamics of membrane lipids in a living cell. *Nature* **457,** 1159–1162 (2009).

32. Digman, M. a, Dalal, R., Horwitz, A. F. & Gratton, E. Mapping the number of molecules and brightness in the laser scanning microscope. *Biophys. J.* **94,** 2320–32 (2008).

33. Otto, A. M., Hintermair, J. & Janzon, C. NADH-Linked Metabolic Plasticity of MCF-7 Breast Cancer Cells Surviving in a Nutrient-Deprived Microenvironment. *J. Cell. Biochem.* **116,** 822–835 (2015).

34. Koppenol, W. H., Bounds, P. L. & Dang, C. V. Otto Warburg's contributions to current concepts of cancer metabolism. *Nat. Rev. Cancer* **11,** 325–337 (2011).

35. DeBerardinis, R. J. *et al.* Beyond aerobic glycolysis: transformed cells can engage in glutamine metabolism that exceeds the requirement for protein and nucleotide synthesis. *Proc. Natl. Acad. Sci. U. S. A.* **104,** 19345–19350 (2007).

36. Vaupel, P., Kallinowski, F. & Okunieff, P. Blood flow, oxygen and nutrient supply, and metabolic microenvironment of human tumors: a review. 6449–6465 (1989). at <http://cancerres.aacrjournals.org/content/49/23/6449.short\npapers2://publication/uuid/971DFCE9-0093-4881-9A0F-7D5CA4C15D78>

Appendix A: Simulations and N&B mathematical background

Simulations

In MatLab R14, using the Optimization and Image Processing Toolboxes, the following simulations were performed. The same spatio-temporal sampling conditions of real acquisitions with the microscope were imposed. Briefly, all populations are set to have the same total number of particles (density of 10 particles/μm^2), with equal quantum yield and randomly seeded in a squared matrix of 64x64 pixels (0.1 μm/pixel). All the simulated acquisitions are $6x10^3$ frames long, with a time step of 10ms/frame; the beam radius is set to 300 nm. Free diffusion and transient confinement (continuum network) were simulated as previously described by others (S3, S4). Each x and y coordinate was changed separately by adding a random number drawn from a normal distribution with a mean of zero, and a standard deviation σ defined as:

$$\sigma = \sqrt{(2D\Delta_t)} \qquad 4)$$

Where D is the diffusion coefficient, and Δ_t is the sampling time between sequential images. In the transient confinement simulation, barriers were simulated as infinitely thin lines that particles can cross with a probability "P", independent of time. In detail, the physical process of crossing the barrier is simplified as follows: when a particle reaches the barrier a random number (rand) is generated between 0 and 1 and compared to P: if rand<P the barrier is crossed otherwise the molecule remains at its previous position (S3). The recovered particle-

position matrix was then convolved with a Gaussian filter to simulate the diffraction-limited acquisition and discretized to a 16 bit integer to simulate a 16 bit A/D converter. Circular boundary conditions for both particle movement and convolution were applied. The contribution of background and counting noises was introduced following the approach described by Kolin et al. (S5). The spatial extension of particles was simulated convolving the particle position with a Gaussian function having a standard deviation equal to the particle size. Averaging of multiple repetitions of the simulations was used to account for longer exposure times.

Number and Brightness: Mathematical characterization of intensity fluctuations

The N&B approach is based in the determination of the first and second moments of the intensity distribution in order to acquire the data at each pixel of an image. In a time series of *K*-values representing counts k_i obtained during the integration time δt , the first and second moments of the distribution of counts are described as follows:

$$\langle k \rangle = \frac{\sum_i k_i}{K}, \tag{14}$$

$$\sigma^2 = \frac{\sum_i (k_i - \langle k \rangle)^2}{K} \tag{15}$$

Where $\langle k \rangle$ is the average and σ^2 is the variance. By acquiring consecutive images in a microscope, these quantities are easily evaluated for any given set of intensity values at each pixel. It is important to note that the integration time at a pixel and the repetition time of the measurement are conceptually different. For instance, images obtained by raster-scan confocal microscopy (as in the case of the present study), each pixel is sampled for a short period of time (in the order of microseconds for the general case), while the same pixel is resampled when the next frame is acquired. Moreover, the pixel dwell time has to be short enough so intensity fluctuations are not averaged out but long enough to capture particle fluctuations.

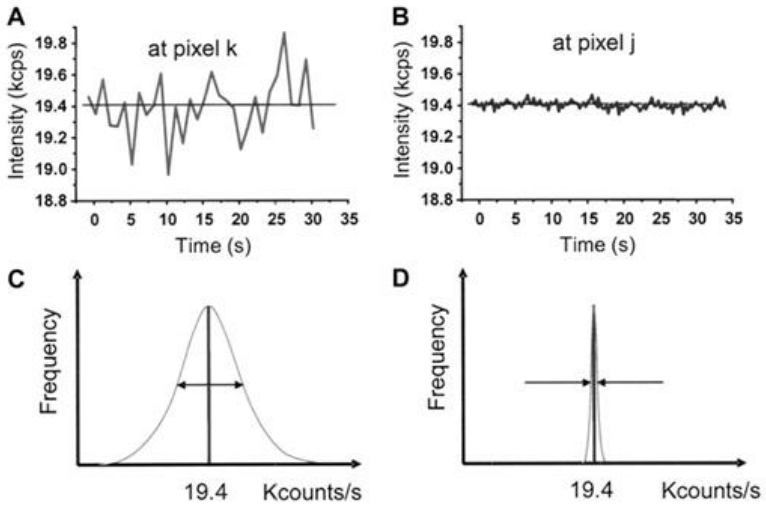

Fig. 22. N&B mathematical background. At pixels *k* (A) and *j*(B) the average intensity is the same but the standard deviation is much larger at pixel *k* in comparison. This is due to few bright particles fluctuating at pixel *k* whereas at pixel *j* there are a large number of dimmer particles. (C) and (D) show schematically the histogram of counts corresponding to the situations in (A) and (B).

Assuming the variance of the intensity measurement is due to the combination of two terms (e.g. the variance due to the count of the occupation number (σ_n^2) and the variance due to the count statistics or shot noise (σ_d^2) of the detector.

These are defined by the following equations:

$$\sigma_n^2 = \epsilon^2 n, \quad (16)$$

$$\sigma_d^2 = \epsilon n \quad (17)$$

$$\langle k \rangle = \epsilon n \quad (18)$$

Eq. 16. States that the variance due to number fluctuations depends on the square of the particle brightness. Eq. 17 states that the detector variance is equal to the intensity and Eq. 18 states that the average intensity is the product of the molecular brightness times the average number of particles.

Therefore, the brightness (B) for each pixel as the ratio of the variance to the average intensity and N (apparent number of particles) as the ratio of the total intensity to B are defined by the following equations:

$$B = \frac{\sigma^2}{\langle k \rangle} = \frac{\sigma_n^2}{\langle k \rangle} + \frac{\sigma_d^2}{\langle k \rangle} = \frac{\epsilon^2 n}{\epsilon n} + \frac{\epsilon n}{\epsilon n} = \epsilon + 1 \quad (19)$$

$$N = \frac{\langle k \rangle^2}{\sigma^2} = \frac{\epsilon n}{\epsilon + 1} \quad (20)$$

The value B is related to the brightness of ϵ particles, and it is independent of the number of particles. N is directly proportional to the number of particles n. It is easy to extract n and ϵ from the above equations:

$$n = \frac{(\langle k \rangle - k_0)^2}{\sigma^2 - \langle k \rangle} \quad (21)$$

$$\epsilon = \frac{\sigma^2 - \langle k \rangle}{\langle k \rangle - k_0} \quad (22)$$